On the Squall Lines Preceding Landfalling Tropical Cyclones in China

ZHIYONG MENG AND YUNJI ZHANG

Laboratory for Climate and Ocean–Atmosphere Studies, Department of Atmospheric and Oceanic Sciences, School of Physics, Peking University, Beijing, China

(Manuscript received 20 December 2010, in final form 17 August 2011)

ABSTRACT

Based on a 3-yr (2007–09) mosaic of radar reflectivity and conventional surface and synoptic radiosonde observations, the general features of squall lines preceding landfalling tropical cyclones (TCs) (pre-TC) in China are examined and compared with their midlatitude and subtropical counterparts. The results show that about 40% of landfalling TCs are associated with pre-TC squall lines with high-occurring frequency in August and from late afternoon to midnight. Most pre-TC squall lines form in a broken-line mode with a trailing-stratiform organization. On average, they occur about 600 km from the TC center in the front-right quadrant with a maximum length of 220 km, a maximum radar reflectivity of 57–62 dBZ, a life span of 4 h, and a moving speed of 12.5 m s^{-1}. Pre-TC squall lines are generally shorter in lifetime and length than typical midlatitude squall lines.

Pre-TC squall lines tend to form in the transition area between the parent TC and subtropical high in a moist environment and with a weaker cold pool than their midlatitude counterparts. The environmental 0–3-km vertical shear is around 10 m s^{-1} and generally normal to the orientation of the squall lines. This weak shear makes pre-TC squall lines in a suboptimal condition according to the Rottuno–Klemp–Weisman (RKW) theory. Convection is likely initiated by low-level mesoscale frontogenesis, convergence, and/or confluence instead of synoptic-scale forcing. The parent TC may contribute to (i) the development of convection by enhancing conditional instability and low-level moisture supply, and (ii) the linear organization of discrete convection through the interaction between the TC and the neighboring environmental system.

1. Introduction

Tropical cyclones (TCs) can produce severe weather conditions not only within its circulation, but also in its ambient environment. Galarneau et al. (2010) analyzed predecessor rainfall events (PRE) appearing about 1000 km poleward of recurving TCs east of a midlatitude trough with the rich moisture supply provided by the landfalling TC. The intent of this study is to document the existence and nature of squall lines preceding landfalling TCs (pre-TC), which are linear mesoscale convective systems (MCSs) that can produce heavy rainfall and damaging winds. These MCSs differ from PREs in that they occur in closer proximity to their parent TC. A prime example of a pre-TC squall line occurred in August 2008 in Guangdong Province of China (see map in Fig. 1) ahead of severe Tropical Storm Kammuri (surface maximum sustained wind speed of 24.5–32.6 m s^{-1}, from the international TC categorization). This squall line (labeled "h" in Figs. 1 and 2) produced rainfall of more than 50 mm; wind gusts of 18 m s^{-1} at Baiyun airport in Guangzhou, China; and caused severe damage to electrical utility poles in Jiangmen, China (its location is marked in Fig. 10g). Another example of a pre-TC squall line occurred in June 2009 when a squall line ("l" in Figs. 1 and 2) ahead of Typhoon Molave brought up to 47.9 mm of rain and wind gusts up to 20 m s^{-1} in Shenzhen, Guangdong province, China. Given their potential severity, it is important to understand the statistical characteristics and dynamics of pre-TC squall lines. However, these squall lines are currently only acknowledged on an empirical observational basis, and their statistical and dynamical characteristics, including comparison with midlatitude and subtropical squall lines, are unknown.

A good reference point to understand pre-TC squall lines is to compare them with their midlatitude and subtropical counterparts. Attributes of midlatitude and subtropical squall lines, such as formation pattern,

Corresponding author address: Dr. Zhiyong Meng, Laboratory for Climate and Ocean–Atmosphere Studies, Department of Atmospheric and Oceanic Sciences, School of Physics, Peking University, 201 Chengfu Rd., Haidian District, Beijing 100871, China.
E-mail: zymeng@pku.edu.cn

DOI: 10.1175/MWR-D-10-05080.1

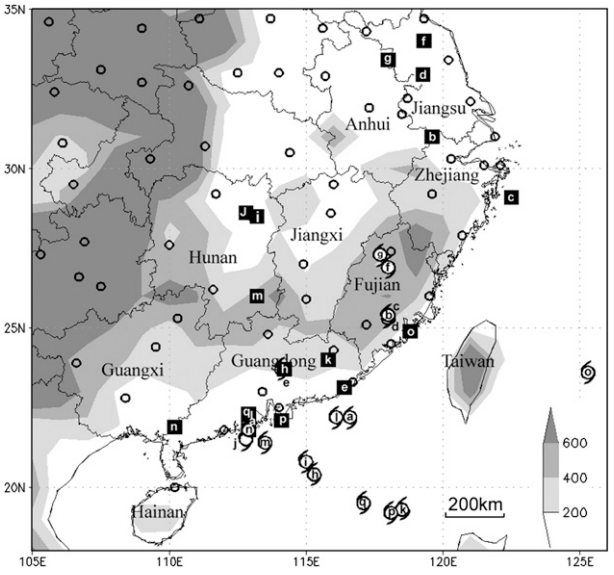

FIG. 1. The locations of Doppler radars (open circles), the midpoints of the leading edge of the 40-dBZ region of pre-TC squall lines at formation (closed squares), and the positions of corresponding tropical cyclone (typhoon marks). The letters inside the closed square and typhoon marks correspond to different parts of Fig. 2 to give a reference to squall-line location. The shading denotes elevation (every 200 m). A horizontal length scale is given in the lower-right-hand corner.

movement, lifetime, and location of stratiform rainfall relative to the linear convection have been well documented (e.g., Bluestein and Jain 1985; Wyss and Emanuel 1988; Houze et al. 1990; Chen and Chou 1993). These studies show that squall lines usually form in environments with large convective available potential energy (CAPE) and low-level vertical wind shear and have been observed near drylines, fronts, or other sources of ascent. We will make extensive comparison between pre-TC squall lines and more kinds of typical squall lines in other environments.

Radar mosaics, which have been widely used in statistical studies of squall lines, are extensively used to accomplish the goals of this study. Past investigations that have used such mosaics include Wyss and Emanuel (1988), who examined radar traits of more than 200 prefrontal squall lines over the contiguous United States from June 1981 to December 1983, and Geerts (1998), who performed a survey of MCS activity in the southeast United States from May 1994 to April 1995. In addition, Parker and Johnson (2000) explored the organizational mode of 88 quasi-linear convective systems in the central United States during May of 1996 and 1997. These works have provided valuable guidance for MCS operational forecast practice, and pre-TC squall-line climatological data should likewise be helpful for TC-associated MCS forecasts and disaster preparedness. Since composite radar mosaics have been available over China only since 2007, results of this work may not have statistical significance due to the small sample size. However, we believe this work sheds some light on the general behavior of pre-TC squall lines.

This paper is organized as follows. Section 2 describes the datasets and methods used. The climatological, structural, and environmental characteristics of pre-TC squall lines are described in section 3. Section 4 presents detailed analysis and numerical experiments of a pre-TC squall-line case, and the concluding discussion is provided in section 5.

2. Data and methodology

Digital radar mosaics of composite radar reflectivity (the horizontal distribution of maximum radar reflectivity in the column) are used in this study to perform the survey. Construction of the Doppler radar network in China began in 1998 as a 10-yr program, and 112 radars were operational in 2007. The distribution of these radar locations in southeast China demonstrates that its coverage (Fig. 1) is adequate to examine the squall lines preceding landfalling TCs.

The regional radar mosaic in southeast China has a time interval of 20 min and a resolution of 4 km $\times$ 4 km. Radar mosaics from June 2007 to October 2009 cover all TCs that made landfall on mainland China during these three years. The radar dataset covers 86% of the sum of time length of all TCs from 24 h before landfall to dissipation or moving out of the radar range. Thus, this dataset is adequate for the survey and examination of pre-TC squall lines.

Using radar reflectivity data, several variants of criteria for defining a squall line have been published in peer-reviewed literature (Table 1). One approach, the dual-reflectivity threshold used by Chen and Chou (1993), defines a squall line when several requirements are met. First, the long axis of a 12-dBZ line of precipitation must be at least 150 km long and exist for at least five continuous hours. Second, the maximum radar reflectivity must reach 36 dBZ with a length–width ratio (LWR) of at least 3:1 at the mature stage. Geerts (1998) used an alternative definition for linear MCSs: 1) the long axis of an area of reflectivity larger than 20 dBZ is at least 100 km and lasts at least 4 h, 2) the region with radar reflectivity larger than 40 dBZ lasts at least 2 h, and 3) the LWR of the 40-dBZ region is at least 5:1. This radar reflectivity threshold seems to be based on the fact that stratiform rainfall is defined where radar reflectivity ranges from 20 to 40 dBZ (Houze 1993), while convective rainfall exceeds 40 dBZ (Steiner et al. 1995).

We use the criteria of Parker and Johnson (2000), which defines a linear or quasi-linear MCS (QLMCS) as

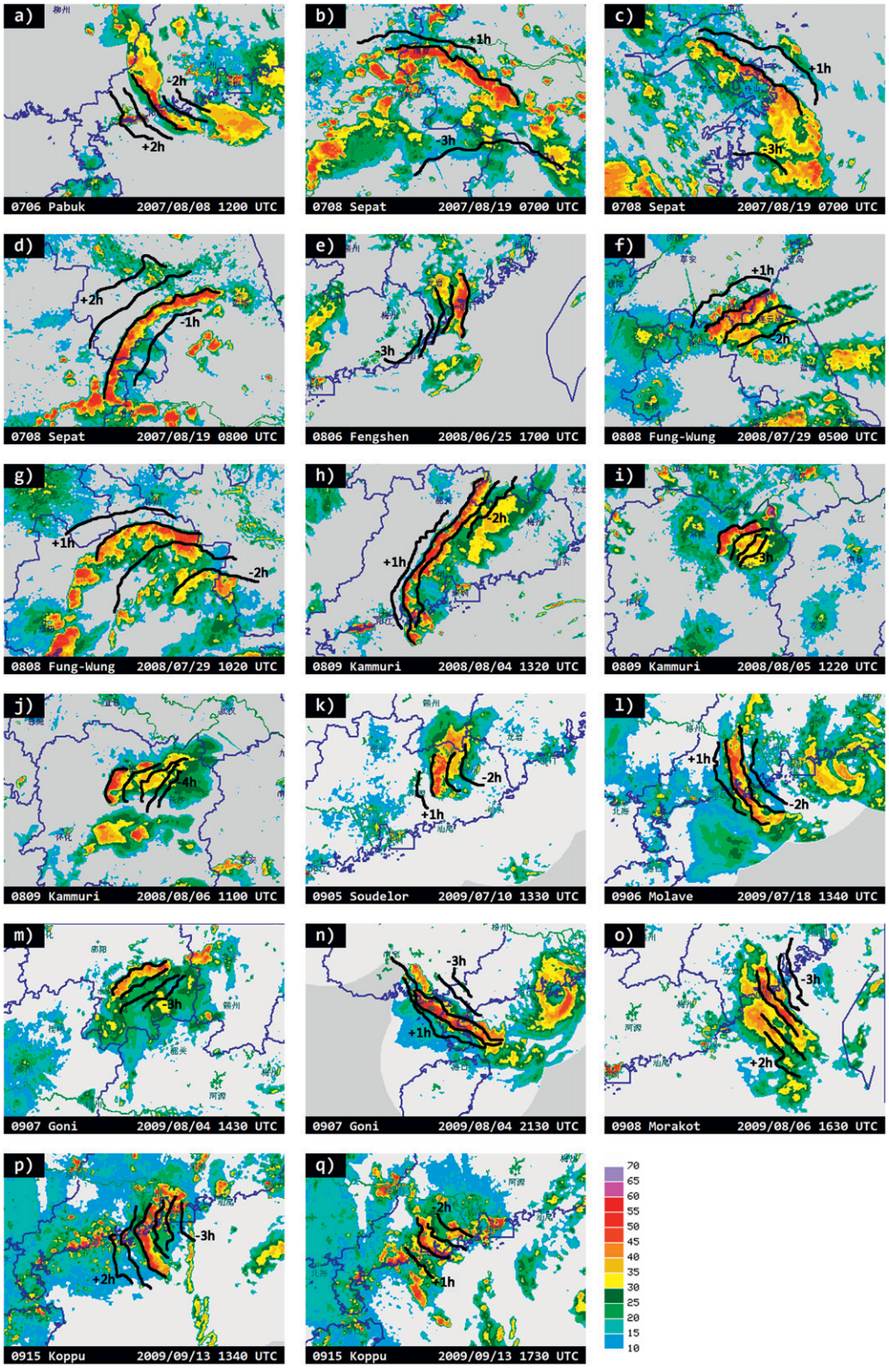

FIG. 2. Composite radar reflectivity (color shaded) of all 17 pre-TC squall lines at their mature stage and isochrones (black solid) at various points during their lifetimes. Information on the bottom includes year, TC number, the name of the TC, and the date and time of the radar mosaic. The numbers of hours before (denoted by −) and after (denoted by +) the plotted reflectivity are also given for the first and last isochrones during their lifetime.

TABLE 1. Several criteria to define linear MCS (squall line) in literature in addition to the pre-TC squall line for this work.

	Chen and Chou (1993)	Geerts (1998)	Parker and Johnson (2000)	Pre-TC squall lines of this work
Data	May–June 1987	May 1994–April 1995	May of 1996 and 1997	January 2007–December 2009
Area	Taiwan and Taiwan strait	Southeast United States	Central United States	Eastern China
Population	6	187	88	17
Criteria	Band of larger-than-12 dBZ ≥150 km and lasts ≥5 h	Band of larger-than-20 dBZ ≥100 km and lasts ≥4 h	Band of continuous or quasi-continuous larger-than-40 dBZ ≥100 km and lasts ≥3 h	As in Parker and Johnson (2000)
	LWR of large-than-36 dBZ band ≥3:1 at mature	Band of larger-than-40 dBZ lasts ≥2 h with a LWR ≥5:1	Linear or quasi-linear convective area sharing a common leading edge	We interpret ''quasi-continuous'' as that we require a 35-dBZ band in which the 40-dBZ convection is embedded in is strictly continuous

a contiguous or quasi-contiguous region of 40-dBZ reflectivity that extends at least 100 km, exists for at least 3 h, and has a linear or quasi-linear convective area with an apparent common leading edge. The ''quasi continuous'' is realized here by requiring that the larger-than-40-dBZ band does not have to be continuous but the 35-dBZ band in which the 40-dBZ line is embedded is strictly continuous. While the requirement of Parker and Johnson (2000) that the quasi-contiguous 40-dBZ band lasts for at least 3 h is a higher standard than that used in previous literature (e.g., Bluestein and Jain 1985; Chen and Chou 1993; Geerts 1998), we chose to use it since they examined several aspects of the linear MCSs including radar traits, organizational structure, and environmental features thus facilitating a more complete comparison. This choice likely limits our sample size because, as mentioned in Geerts (1998), slightly increasing the lower-reflectivity thresholds may rapidly trim the database, which suggests that there is a fairly distinct tail in the distribution of reflectivity values in MCSs. Since the collection of radar mosaic of the 0.5° base scan is unavailable for a long term, the use of composite radar reflectivity makes our criterion somewhat weaker than that of Parker and Johnson (2000). This weaker criterion may result in a larger sample size.

We differentiate pre-TC squall lines from TC rainbands following Powell (1990), who briefly compared outer hurricane rainbands to tropical squall lines. First, Powell (1990) noted that squall lines propagate at a much faster speed than do outer hurricane rainbands. In addition, convection is located on the inner or trailing side of TC rainbands, while it is usually located on the leading edge of a squall line. For our purposes, we add criteria that the 20-dBZ region must be clearly separated from the main body of the associated TC, and that the squall line must cross the front quadrant(s) relative to the TC track. There are linear convective lines with a 40-dBZ band longer than 100 km moving into the radar range from the sea. However, none of them lasts more than 3 h after being observed on radar images. Since we have no way to know how long they have sustained before entering in the radar range, these cases were not counted. Radar traits of thus-determined pre-TC squall lines are defined in Table 2.

In addition to the above radar traits, the formation mode is assigned one of four basic modes defined by Bluestein and Jain (1985). These include broken lines (BL; new cells develop between old cells and merge with them to form a contiguous or quasi-contiguous line), backbuilding (BB; new cells form serially at the back of original cells and merge with them and form a line), broken areal (BA; a convective band forms among scattered cells), and embedded areal (EA; a convective band forms in a widespread stratiform region). We will use the dominant mode to represent the formation of a particular pre-TC squall line.

Finally, the organizational mode falls into one of three basic categories proposed by Parker and Johnson (2000). These modes, which are defined according to the juxtaposition of stratiform and convective rainfall, include leading (LS), trailing (TS), and parallel stratiform (PS). As with formation, the dominant mode will be used to represent the organizational type.

3. Characteristics of squall lines preceding landfalling TCs

a. Spatial and temporal distribution

During 2007–09, a total of 23 TCs made landfall on mainland China. Based on our thresholds, 17 squall lines

TABLE 2. Definition of various radar traits of pre-TC squall lines.

Radar traits	Definitions
Formation time	When the pre-TC squall-line threshold is first met
Dissipation time	When the pre-TC squall-line threshold is continuously last met for more than 3 h after its formation
Lifetime	During which the pre-TC squall-line threshold is continuously met
Max length	The length of the maximum straight long axis of quasi-contiguous 40-dBZ reflectivity band
Mature time	The time when the maximum length is achieved
Speed	The length of a line connecting the midpoints of the hourly isochrones at the leading edge of the quasi-linear 40-dBZ band during the lifetime divided by the lifetime
Intensity	The maximum value of radar composite reflectivity during the lifetime

were observed preceding 10 landfalling TCs. This result suggests that about 43% of landfalling TCs during this period are associated with pre-TC squall lines. Figure 1 shows the formation location of each squall line with a filled square and the corresponding TC position with a typhoon mark that has the same letter as that in the filled square. The radar reflectivity during the mature stage of each squall line and isochrones at various points of the lifetime are presented in Fig. 2. One interesting result is that half of the landfalling TCs associated with pre-TC squall lines were actually accompanied by multiple squall lines. For example, three pre-TC squall lines (denoted by h, i, and j in Fig. 1) occurred during the lifetime of TC Kammuri (2008). This phenomenon is probably due to the lasting of an environment that is favorable for the formation of squall lines under the interaction between the parent TC and its ambient systems as demonstrated later on. Among the 17 squall lines, seven formed in Guangdong Province, and the others appeared in Guangxi, Fujian, Hunan, Jiangxi, Zhejiang, Anhui, and Jiangsu Provinces (refer to Fig. 1 for their locations). All squall lines formed over relatively flat topography, which is consistent with distribution of warm season rainfall in north China (He and Zhang 2010).

The highest frequency of pre-TC squall lines appeared in August (Fig. 3a), which is close to the peak frequency of landfalling TCs. The pre-TC squall lines during the period of this study formed mostly from late afternoon to midnight (Fig. 3b), which is consistent with the nocturnal maximum of thunderstorms (Wallace 1975) and linear MCS activity over the United States (Geerts 1998; Parker and Johnson 2000).

b. General radar traits

About 35% of the pre-TC squall lines were 200–250 km long (Fig. 3c), and the average maximum length was 224 km, which is close to the average maximum length of subtropical squall lines associated with mei-yu front in China (230 km in Chen and Chou 1993). About 60% of the squall lines were longer than 200 km. The maximum intensity had a range of 55–65 dBZ with an average of 57–62 dBZ (Fig. 3d), which is about 5–10 dBZ higher than the averaged maximum dBZ of outer Hurricane rainbands (H. Jiang 2010, personal communication). The mean lifetime of the pre-TC squall lines studied here was 4 h (Fig. 3e), which is shorter than that of midlatitude squalls in the central United States (i.e., 6–12 h; see Parker and Johnson 2000) and subtropical squall lines (i.e., 11.4 h in Chen and Chou 1993).

Many similarities were found between pre-TC and midlatitude squall lines. For example, most pre-TC squall lines observed here moved with a mean speed of 12.5 m s^{-1} (Fig. 3f). This is similar to squalls associated with the mei-yu front in China (Chen and Chou 1993) and MCSs in the central United States (Parker and Johnson 2000). The squall-line motion vector was approximately perpendicular to the orientation of the pre-TC squall lines, which has been also observed in subtropical squall lines associated with the mei-yu front (Chen and Chou 1993) and prefrontal squall lines in the United States (Wyss and Emanuel 1988).

The maximum length, life span, and moving speed of pre-TC squall line were also compared to those of squall lines in north China. Li (1988) analyzed features of 10 squall lines in north China during 1970–80 using surface observations. They found that the dominant length, life span, and moving speed were 200–300 km, 3–10 h, and 14 m s^{-1}, respectively. Relative to the north China squall lines, pre-TC squall lines seem to have a comparable length with a shorter life span and a slower moving speed.

Also similar to the midlatitude prefrontal squall lines, a majority (about 70%) of the pre-TC squall lines formed in broken-line mode (Fig. 3g; Bluestein and Jain 1985; Houze et al. 1990; Parker and Johnson 2000). Three were found to form by broken areal, and two

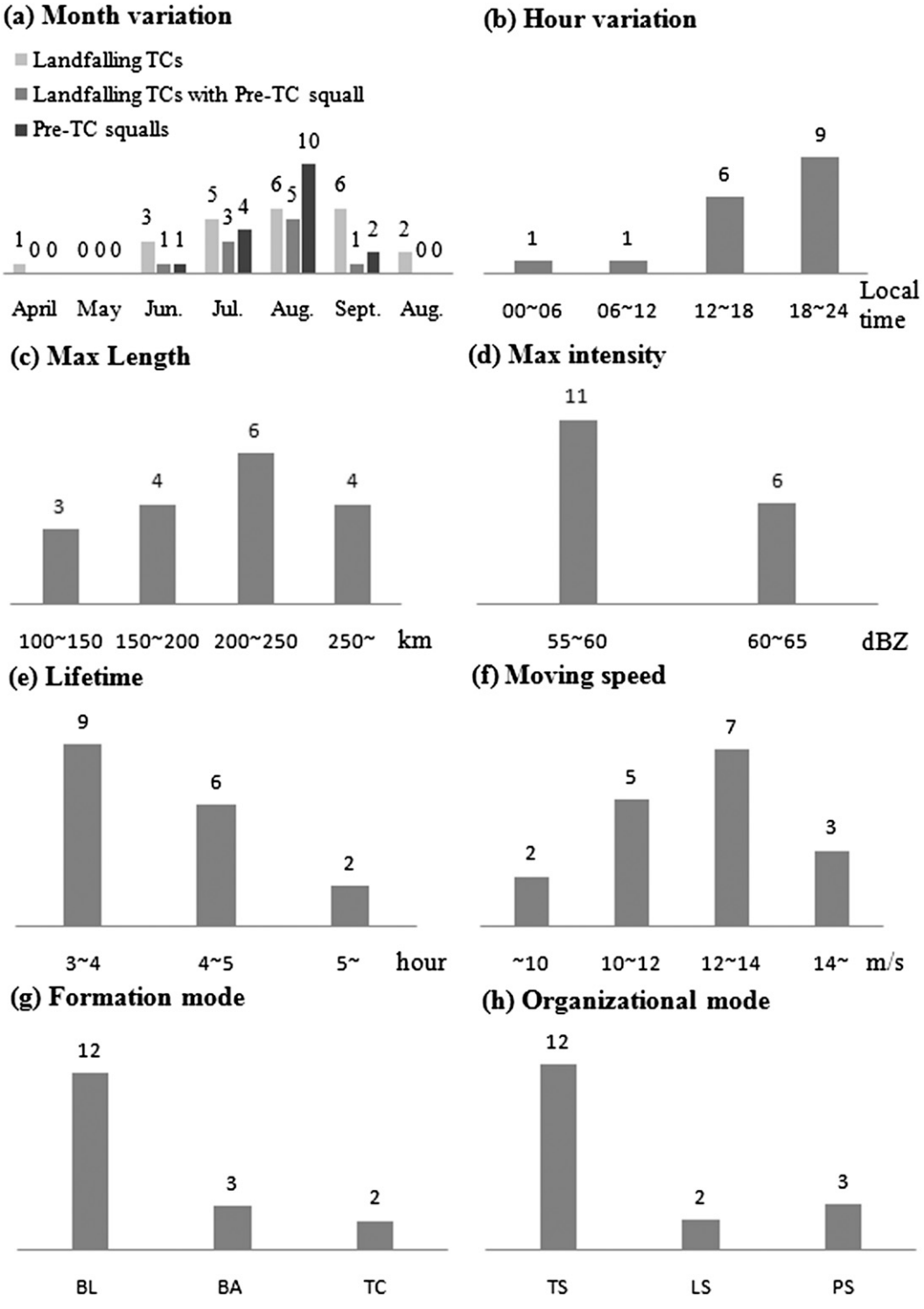

FIG. 3. The numbers of pre-TC squall lines appearing (a) in different months, (b) during different periods of a day, with different ranges of (c) maximum length, (d) maximum intensity, (e) lifetime, (f) moving speed, (g) formation mode, and (h) organizational mode.

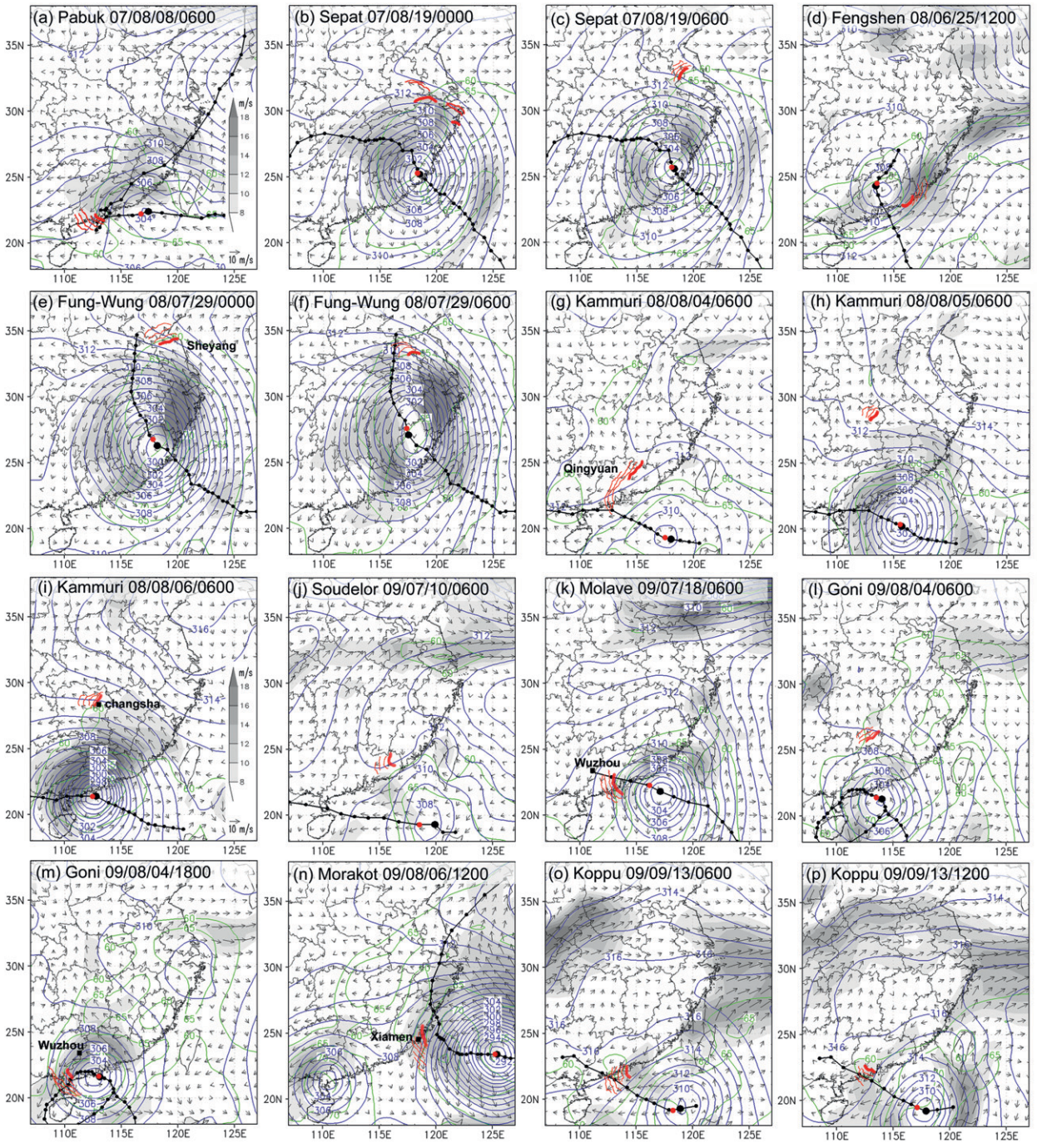

FIG. 4. (a)–(p) The FNL/NCEP analysis on geopotential height [every 10 geopotential meters (gpm)] at 700 hPa, column-integrated precipitable water larger than 60 kg m^{-2} (green contour every 5 kg m^{-2}), as well as the vertical shear vector and magnitude (shaded, every 2 m s^{-1}) between 700 and 1000 hPa [the representative wind vector is given in the lower-right corners in (a) and (i)] at the time [year/month/day/time (UTC)], and for the tropical cyclone as given by the subtitles. The isochrones of their pre-TC squall lines are plotted in red. The red dot on the track denotes the position of the TC when its preceding squall line forms as indicated by the heavy red line, which is within 6 h after the time of the plotted FNL/NCEP analysis as given in the subtitle.

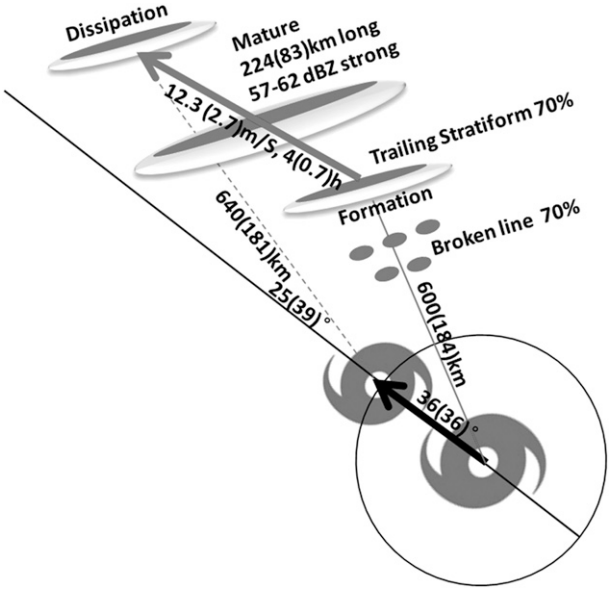

FIG. 5. Schematic diagram of the averaged features of pre-TC squall lines. The number in parentheses is the corresponding standard deviation.

began as TC rainbands but transitioned into squall lines. The organizational mode of pre-TC squall lines were also examined (Fig. 3h). Twelve out of the 17 cases had a trailing-stratiform structure, 2 had leading stratiform, and 3 had parallel stratiform. Transition zones were observed in four cases with trailing stratiform. The dominance of trailing-stratiform organization is similar to midlatitude squall lines in the United States (Parker and Johnson 2000), and more importantly differentiates these pre-TC squall lines from the outer rainbands of TCs since the outer rainbands mainly have leading stratiform with the convective rainfall appearing inward of the band (Powell 1990).

c. Relationship to the parent TC

This section examines pre-TC squall lines in relation to their associated TCs. Figure 4, which shows the isochrones of each squall line and the tracks of their respective TC, demonstrates that the pre-TC squall lines tend to form in the front-right quadrant of the TC. Note that squall line may also occur in the back quadrants of the TC, here we just focus on those in the front quadrants thus their tendencies to form in front-right quadrant is dependent of our squall-line identification method. While our small sample size inhibits examination of the impacts of TC track, size, and intensity, Fig. 4 does show that pre-TC squalls occurred in TCs wherein these parameters varied considerably. The tracks of the 10 TCs documented here varied from westward to northward, and although most TCs were weakening, there were still cases when a pre-TC squall line accompanied an intensifying TC. In addition, squall lines with larger TCs tended to be farther from the TC center. More detailed analysis on how TC size and intensity affects pre-TC squall lines will be discussed in a case study in section 4.

A schematic diagram illustrating average features of pre-TC squall lines over the 17 cases is represented in Fig. 5. The oblong band with leading dark gray denotes a line with dominant trailing-stratiform organization that has formed via a dominant broken-line mode (denoted by cells). On average, these lines formed about 600 km ahead of the TC center and 36° to the right of the TC trajectory with standard deviations of 184 km and 36°, respectively. They typically moved more quickly than the TC and therefore dissipated farther from the TC center than when they originated.

d. Surface features

This section uses hourly surface observations [from surface mesoscale observing network of China provided by the real-time dataset of the China National Meteorological Center (CNMC)] to examine the strength of cold pools and pressure and wind changes caused by the passage of pre-TC squall lines. As in Engerer et al. (2008) and Evans and Doswell (2001), we use the perturbation of surface potential temperature before and after the gust front passes a station to estimate the strength of the cold pool. The differences between extreme values of potential temperature, mean sea level pressure (SLP), and 10-m wind direction and speed were calculated within 2 h of the sharpest rate of change in surface potential temperature. The two stations with the highest potential temperature drop in each pre-TC squall-line case are used to calculate the distribution of corresponding pressure rise, potential temperature drop, changes of wind direction and speed, as well as the maximum 1-h rainfall displayed in the box and whisker plots in Fig. 6. According to our statistics, the pre-TC squall line has an averaged rain rate of 18 mm h^{-1}, with a maximum measured value of 65 mm h^{-1}. Though pre-TC squall lines have a high rain rate, they usually do not directly cause severe flooding since they move rapidly and their life span is generally short (around 4 h). They may contribute indirectly to the flooding, however, by saturating the soils prior to the arrival of the TC rain shield as can occur with PREs (Galarneau et al. 2010). The primary threat associated with pre-TC squall lines are strong straight-line winds.

Though these cases were accompanied by heavy rain and dramatic wind shifts, their cold pools appeared to be somewhat weaker than those of midlatitude MCSs. The passage of the squall lines featured wind shifts ranging from 20° to 180° with a median of 80° and a median of the

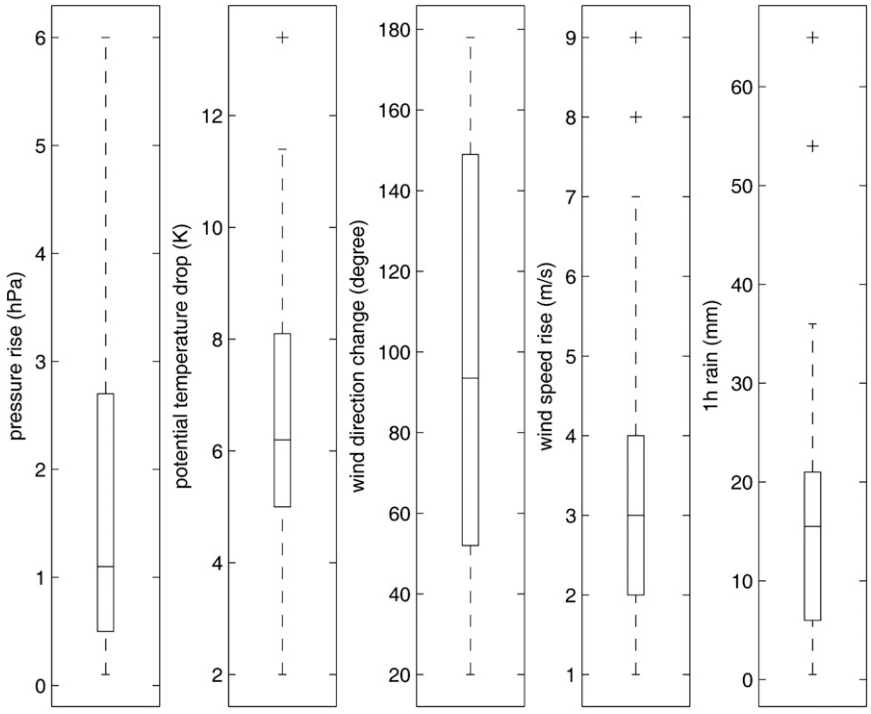

FIG. 6. Box-and-whisker plot of the changes of surface variables during the passages of all the 17 pre-TC squall lines including the pressure rise, potential temperature drop, changes in wind direction, increase in wind speed, and the observed 1-h rainfall. The box-and-whisker plots show the median (short line in the box), interquartile range (rectangle), and outliers (i.e., the 10th and 90th percentile as whiskers) for the indicated variables.

maximum 1-h rainfall of about 17 mm. The decrease in surface potential temperature ranged from 2 to 13.4 K with a median of 6.2 K. Though the range in potential temperature drop was similar to midlatitude systems, the median was smaller than that associated with derechos (a median of 8 K in Evans and Doswell 2001) or midlatitude MCSs (a median of 9.8 K in Engerer et al. 2008), or the average of the temperature decreases reported from convective systems in literature (8.9 K in Engerer et al. 2008). The maximum decrease of surface potential temperature was 13.4 K for the pre-TC squall-line cases, which is about 4 K less than the maximum decrease of surface potential temperature observed in the 39 MCSs in Oklahoma during 2000–07 (Engerer et al. 2008).

Changes in surface pressure across the squall lines were consistent with their weaker cold pools. The pressure rise ranged from 0.2 to 6 hPa and had a median of 1.2 hPa. Similar to the perturbation of potential temperature, the pressure rise had a similar range, but a much smaller median relative to that of MCSs in Oklahoma (4.5 hPa in Engerer et al. 2008) and the mean of the values reported in literature (3.6 hPa in Engerer et al. 2008). The maximum pressure rise was 6 hPa, which is also smaller than 9.4 hPa reported in Engerer et al. (2008). The weaker cold pool is also suggested by the small changes of wind speed, though the corresponding statistics for midlatitude squall lines are not available for comparison. Note that wind gust data is unavailable for the long-term period, and the use of 2-min-average wind of surface observation results in smaller wind speeds.

e. Environment features

Conventional radiosonde data from the University of Wyoming (available online at http://weather.uwyo.edu/upperair/sounding.html, which is based on the conventional radiosonde network of CNMC) is used to examine the environments of pre-TC squall lines. Soundings released within 6 h before the passage of a squall line and uncontaminated by convection are used to analyze the presquall environment. Since the conventional radiosondes are very coarse in both temporal and spatial distribution, only six soundings meet the criteria. These six soundings are used to assess characteristic of the environment associated with pre-TC squall lines (Fig. 7).

Low-level vertical shear has long been recognized as an important role in the development and evolution of

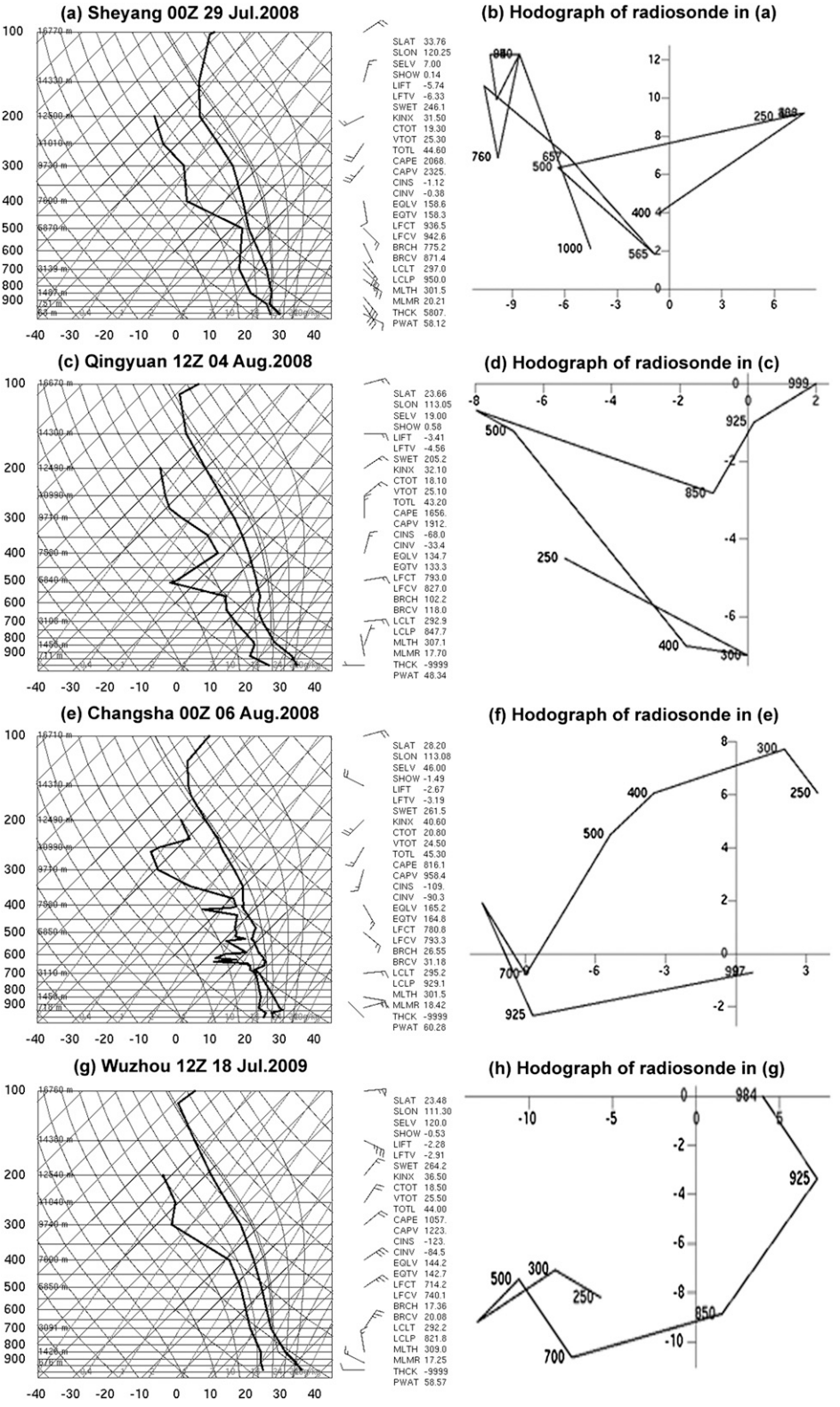

FIG. 7. (a)–(l) Radiosondes and hodographs (m s^{-1}) representing the environments in front of the pre-TC squall line as marked in Figs. 4e,g,i,k,m,n. (Available online at http://weather.uwyo.edu/upperair/sounding.html.)

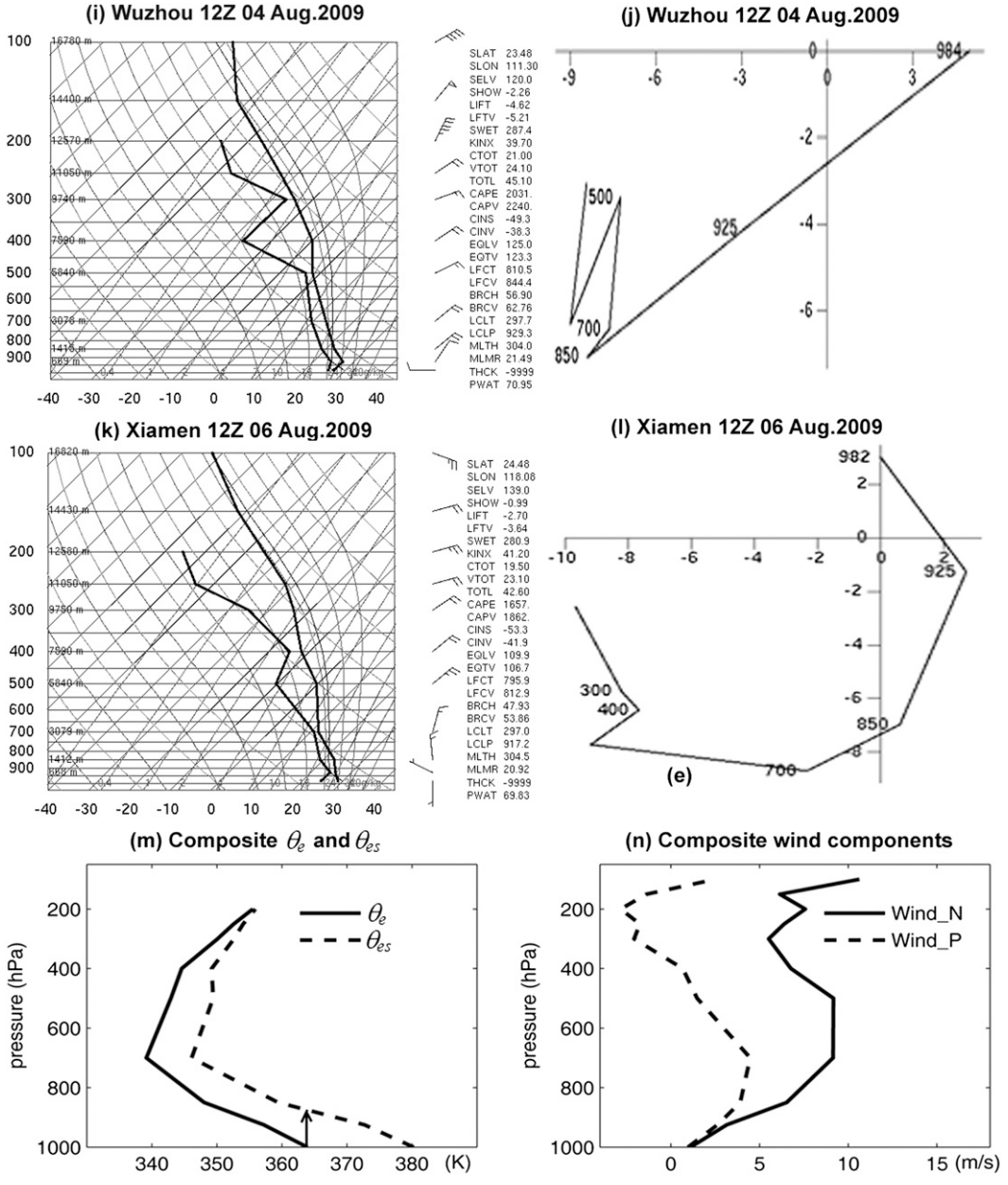

FIG. 7. (*Continued*) The locations of the respective radiosonde stations are denoted by the solid square in Fig. 4. The wind barbs on the right-hand side of the radiosonde are in the unit of kt (A full line on the wind barb is 10 kt, a half line is 5 kt, and a flag is 50 kt, where 1 kt = 0.5144 m s^{-1}). Also shown are the composite profiles of (m) equivalent potential temperature θ_e (solid) and saturation equivalent potential temperature θ_{es} (dashed) and the wind component (n) normal (solid) and parallel (dashed) to the long axis of pre-TC squall lines. The arrow in (m) indicates the rising of an air parcel with surface θ_e.

squall lines (Rotunno et al. 1988). The environments in front of the pre-TC squall lines show a generally consistent low-level veering wind (also clearly shown in corresponding hodograph in Fig. 7), indicating a warm air advection and attendant quasigeostrophic forcing for ascent. The 0–3-km vertical shear is about 8 m s^{-1}, which is smaller than that of subtropical squall lines (10–14 m s^{-1} in Chen and Chou 1993) and midlatitude squall lines (Rotunno et al. 1988). The 0–3-km vertical shear vector is mostly normal to the long axis of the pre-TC squall lines pointing toward their moving direction, which is consistent with previous studies on tropical squall lines (e.g., Houze 1977; Barnes and Sieckman 1984). The dominant 0–3-km vertical shear normal to the long axis

of squall line, rather than parallel, is clearly shown in the composite vertical profiles of the two wind components of the six soundings (Fig. 7n). These features of low-level vertical shear are also clearly shown in the final analysis (FNL) of the National Centers for Environmental Prediction (NCEP; Fig. 4). The 1000–700-hPa vertical shear is around 10 m s^{-1} and approximately normal to the orientation of the pre-TC squall line in 88% of the cases, which is generally beneficial for the development of linear convection (Rotunno et al. 1988; James et al. 2005). The dominant low-level vertical shear normal to the squall line is consistent with previous studies on fast-moving tropical squall lines (e.g., Barnes and Sieckman 1984), subtropical (e.g., Chen and Chou 1993), and mid-latitude (e.g., Bluestein and Jain 1985; Wyss and Emanuel 1988) squall lines.

The averages of the derived properties of these six soundings are listed in Table 3 in comparison to results of previous literature. The mean CAPE (1548 J kg^{-1}) is less than that associated with spring squall lines in Oklahoma (Bluestein and Jain 1985) and linear MCSs with trailing stratiform in the central United States (Parker and Johnson 2000). However, it is the stronger-than-average CAPE ahead of squall lines over the entire contiguous United States (Wyss and Emanuel 1988) and subtropical squall lines associated with mei-yu front in China (1340 J kg^{-1} in Chen and Chou 1993). The larger CAPE of pre-TC squall lines relative to subtropical squall lines (Chen and Chou 1993) can also be clearly seen from the larger area delineated by the surface equivalent potential temperature larger than the saturation equivalent potential temperature in the vertical (Fig. 7m; also see Fig. 6 in Chen and Chou 1993). On the other hand, convective inhibition (CIN) was larger than that of Bluestein and Jain (1985), but smaller than that of Wyss and Emanuel (1988). The lower level of free convection (LFC) of pre-TC squall lines relative to that of subtropical squall lines (Fig. 7m; see Fig. 6 in Chen and Chou 1993) indicates that pre-TC squall lines may have a smaller CIN than subtropical squall lines.

The environment of pre-TC squall lines also had much higher precipitable water (PW) and a slightly lower lifting condensation level (LCL) relative to that in Parker and Johnson (2000) and Bluestein and Jain (1985). The PW is near 60 kg m^{-2} in most cases of the pre-TC squall lines (Fig. 4). This big difference in PW is likely a reflection of the climatological difference between the near-maritime environment of pre-TC squall lines and the inner continental environment of the aforementioned midlatitude cases. Rich moisture supply from the approaching TC may have additionally enhanced the PW, as will be suggested by the case study in section 4. The importance of water vapor supply from the associated TC has also been shown to be a key component for PREs by Galarneau et al. (2010) and Schumacher et al. (2011).

TABLE 3. Comparison between averages of derived properties of the environmental soundings in front of squall lines in different studies. LI: Lifted index.

Avg of derived properties	CAPE (J kg^{-1})	CIN (J kg^{-1})	LI (K)	LCL (hPa)	PW (cm)
Pre-TC squall lines	1548	67	−3.6	899	6.1
Bluestein and Jain (1985)	2260	33			2.8
Parker and Johnson (2000)	1605		−5.4	831	3.4
Wyss and Emanuel (1988)	1208	76			

To get a general picture on possible impact of the environment on the formation of the pre-TC squall lines, we performed a composite analysis in a similar way as that in Galarneau et al. (2010) with the first squall lines associated with each of the nine landfalling TCs that have westward motion component (TC Fengshen in Fig. 4d was excluded because of its eastward motion component and the differing environmental pattern from others). The composite analyses were produced with respect to TC at $T - 12$ h, $T - 6$ h, T, and $T + 6$ h in which T denotes the formation time of the squall lines (Fig. 8). In particular, we first determined the median of all the 9 TCs, and then shifted the FNL analyses so that the TC centers overlap the median location. After that, averages of different variables were computed. The composite analysis shows an apparent moisture increase toward the formation position of the squall line obviously due to the transportation through the outer flow of the approaching TC. The squall line tends to form in the transition area between the TC and subtropical high where low-level Petterssen frontogenesis intensified approaching to the formation of the squall line and weakened as the squall line dissipates.

To further examine the difference between the landfalling TCs that produce pre-TC squall lines and those that do not, we produced composite analyses for those 13 TCs that are not associated with preceding squall lines with respect to the TC at 18 and 6 h before landfall (Figs. 8e,f). Comparing with the TCs that have preceding squall lines at a similar distance from the costal line (Figs. 8a,c), we found that the TCs without preceding squall lines are drier with the precipitable water of larger than 60 kg m^{-2} limited only near the TC center. Both the TC and the subtropical high are located more to the south since most TCs without preceding squall lines occur before July or after August (Fig. 3a). The subtropical high is stronger and oriented more longitudinal. The flow between the TC and the subtropical high is more southerly compared to the pre-TC squall-line composite. As a result, the moisture flux into China and the convergence

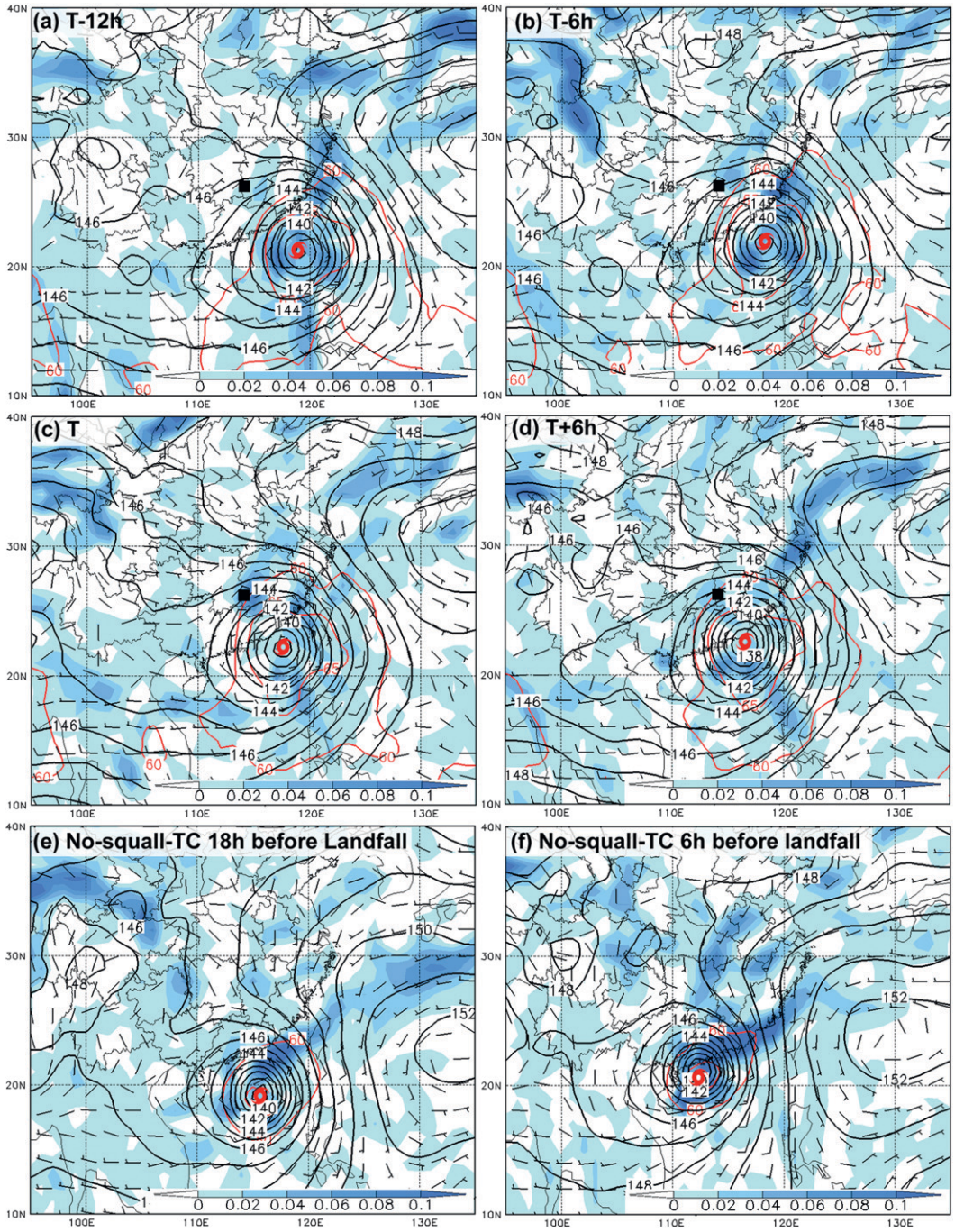

FIG. 8. Composite analysis of 925-hPa frontogenesis [10^2 K km^{-1} (3 h)$^{-1}$; shaded], 850-hPa geopotential height (black contour every 10 gpm), and wind vector (full barb =10 m s^{-1}) as well as column-integrated precipitable water (red contour every 5 kg m^{-2}) for the 9 cases that have a westward motion component during 2007–09 at (a) −12, (b) −6, (c) 0, and (d) 6 h relative to the formation time T of pre-TC squall line. The solid square denotes the median of the formation locations of the 10 pre-TC squall lines at time T. The red TC mark denotes the TC center. (e),(f) As in (a)–(d), but for the TCs that are not associated pre-TC squall lines at 18 and 6 h before landfall.

along its coastal line are reduced. Likely associated with this juxtaposition, the frontogenesis in the transition area between the TC and the subtropical high is weaker. The reduced moisture supply, thus also the reduced instability and the weakened ascent due to weakened low-level convergence, likely led to the lack of pre-TC squall lines. This result indicates that the formation of pre-TC squall lines could be closely related to the rich moisture supply by the

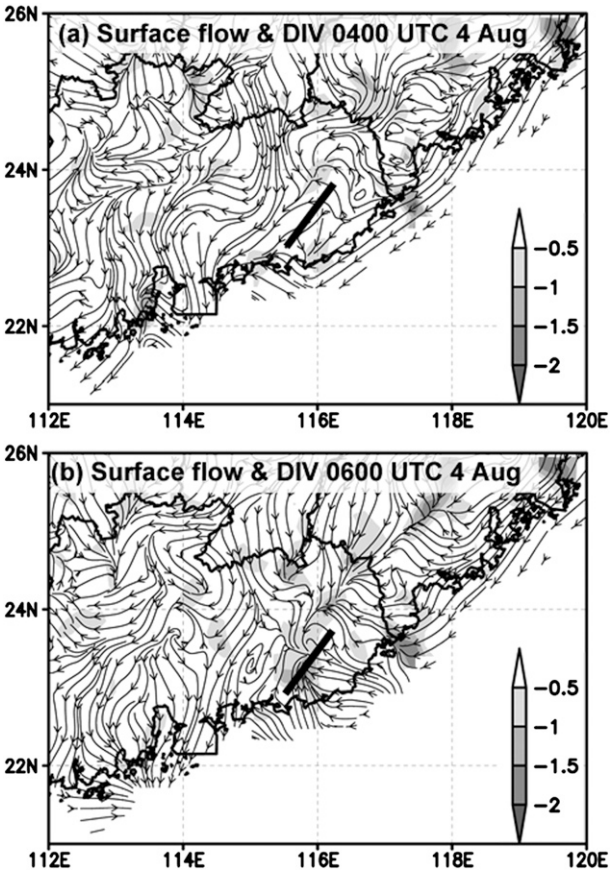

FIG. 9. Surface flow and convergence (shaded; 10^{-4} s^{-1}) at (a) 0400 and (b) 0600 UTC 4 Aug 2008. The short heavy line represents the orientation of linear growth of initial convection.

associated TC as well as low-level convergence and the associated low-level frontogenesis.

As demonstrated by Dial et al. (2010), low-level linear convergence is often associated with the rapid upscale linear growth of discrete convection. To examine how the initial convection evolves into a squall line, the hourly surface flow around the development of the initial convection with composite radar reflectivity larger than 40 dB*Z* was analyzed. In each case over land, quasi-linear surface confluent flow with increasing convergence was observed around where the initial convection was organized into a line shortly thereafter. An example of the evolution of the surface convergence and confluence for TC Kammuri (2008) is shown in Fig. 9. A linear surface confluence was present near the coastal line of Guangdong Province early at 0400 UTC 4 August, which is about 2 h earlier than the initial convection near the southern end of the heavy line in Fig. 9a. Two hours later, the confluent line became longer extending all the way to Fujian Province (Fig. 9b). The confluent line was collocated with an apparent linear convergence band. About 40 min later, the convection was initiated and rapidly grew upscale into a convective line oriented in the same direction as the confluent line. The intensification and extension of the confluent line is likely due to the enhancement of onshore flow especially to the east of 115°E. This result indicates that the approaching TC may not only provide rich moisture for convection initiation, but also facilitate the upscale linear growth of the convection into a squall line. The impact of Kammuri on the formation and evolution of its associated pre-TC squall line is examined in more detail in the next section.

4. The case of a squall line preceding severe Tropical Storm Kammuri (2008)

To provide a clearer picture of the behavior of pre-TC squall lines and the possible impact of the TC on the preceding squall line, a case associated with severe tropical storm Kammuri in August 2008 is described in more detail in this section. Kammuri formed as a tropical depression at 1200 UTC 3 August 2008 near the Philippines (Fig. 4g). During its lifetime, Kammuri was associated with three pre-TC squall lines (Figs. 2h–j and 4g–i). Here we examine the first one with a well-developed structure, which formed while Kammuri was still a tropical depression (Figs. 2h and 4g).

a. Kammuri's squall line

The first echo of radar reflectivity associated with the squall line was observed at 0640 UTC 4 August 2008 (identified by the red open circle in Fig. 10a). In the very beginning of the development, the convective band formed through a broken-line mode (Figs. 10a–c). Later on, a new longer band formed in front of the first band also in a broken-line pattern (Figs. 10c,d). The new band eventually became the leading edge of the squall line, while the original convective band developed into a trailing-stratiform region (Figs. 10e,f). The stratiform precipitation was mainly observed in northern part of the line, which contributed to an asymmetric structure as described by Houze et al. (1990).

The squall line reached its maximum length of 500 km and maximum intensity of 60–65 dB*Z* at 1342 UTC 4 August. It moved toward west-southwest at a speed of about 11 m s^{-1} and lasted for 3.7 h. The dissipation started with the weakening of the leading convective line and followed with gradual shrinking of the trailing-stratiform rainfall.

Changes in surface observations typically associated with squall lines were observed. Qingyuan (refer to its location in Fig. 10g) station received an hourly precipitation maximum of 20 mm, recorded a pressure jump of 5 hPa, a temperature drop of 7 K, a wind speed

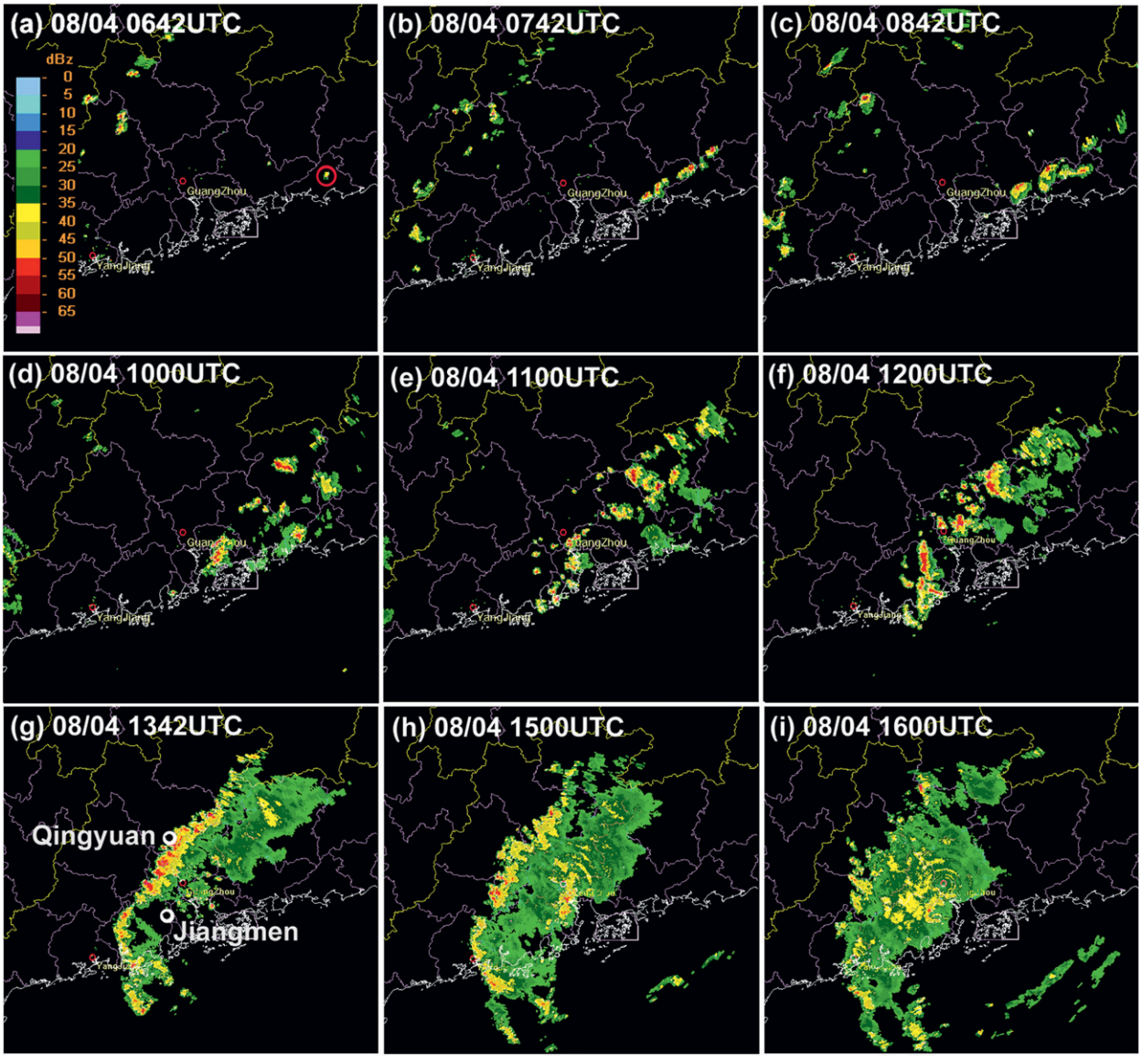

FIG. 10. The evolution of composite radar reflectivity of a squall line associated with severe tropical storm Kammuri on 4 Aug 2008. (a) The first observed convection is the one in the open circle.

increase of 5 m s^{-1} and an abrupt change of wind direction during the passage of the squall (Fig. 11). The surface structure was well developed with an apparent cold pool, storm high (H in Fig. 11b), prelow (L in Fig. 11b), and wake low.

Synoptic analysis was performed to examine the environmental features during the formation of the pre-TC squall line. During the 6 h before the formation of the pre-TC squall line, a 200-hPa trough near (25°N, 116°E) retreated northward and westward (Figs. 12a,b). The westward movement of the trough can be clearly seen from the distribution of potential temperature and wind on the dynamic tropopause (Figs. 12c,d). Convection was initiated right at the base of the trough (heavy solid line in Fig. 12b). This result indicates that the upper-level trough may have helped to increase CAPE by providing cooling aloft. Since the convection was initiated on the left entrance of the 200-hPa jet on the east flank of the trough (the wind band on the west flank is too weak to be counted as a jet), the upper-level forcing for ascent on the synoptic scale may be unimportant in the development of the convection. This feature is apparently different from PRE in which the synoptic forcing for ascent by the upper-level jet plays an essential role (Galarneau et al. 2010; Schumacher et al. 2011). The priming role of the synoptic-scale forcing is further confirmed by the analysis of the

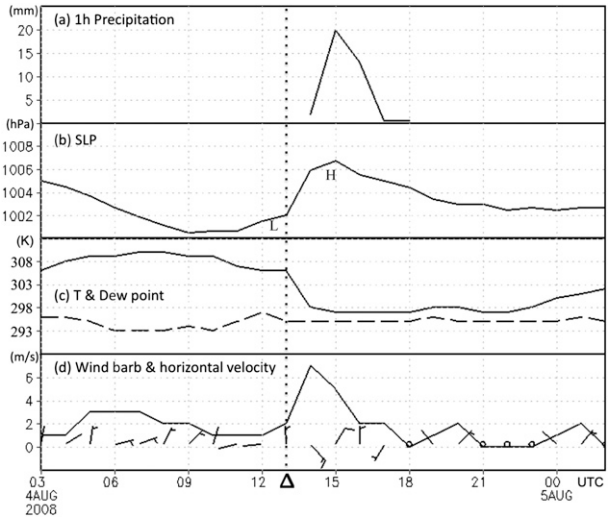

FIG. 11. Variation of surface variables including (a) hourly precipitation, (b) sea level pressure (L and H denote the prelow and mesohigh), (c) temperature (solid) and dewpoint (dashed), and (d) wind barbs (full barb = 5 m s^{-1}) and horizontal velocity when the pre-TC squall line associated with severe TS Kammuri passed over Qingyuan, Guangdong Province, during 0300 UTC 4 Aug–0000 UTC 5 Aug 2008. The location of Qingyuan station is marked by a white open circle indicated by its name in Fig. 10g.

quasigeostrophic (QG) omega equation. Following the same method used in Gao et al. (2009), we computed the two forcing terms on the right-hand side of the QG-omega equation and also the difference between the absolute values of the two terms: forcing from vorticity advection and temperature advection (Figs. 13a,b). The result shows that the forcing for ascent associated with vorticity and temperature advection are comparatively weak at 0000 UTC 4 August. The warm-air advection term intensifies and dominates vorticity advection term 6 h later. This result indicates that QG forcing for ascent may have helped to increase the CAPE and decrease the CIN, thus destabilizing the environment. The increasing low-level convergence (Fig. 9) and frontogenesis (Figs. 13c,d) with the associated intensifying baroclinicity during this period are shaped in a more similar way to the orientation of the main axis of the initial convection, thus, this may have more directly forced the initiation of the convection. The pre-TC squall line also appears in front of a 925-hPa inverted trough of the TC, which is consistent with the previous literature on the synoptic environmental analysis of squall lines in China (Ding et al. 1982). This inverted trough intensifies the onshore flow thus helps to enhance the low-level confluent flow.

Kammuri may have played an important role in the formation of the squall line. Its contribution to the convection initiation can be clearly identified from the advection of a moist air mass into the region of convective initiation (shaded in Figs. 14a,b) through the intensifying cyclonic flow around the developing TC. This moisture transportation is demonstrated more clearly in a 48-h backward trajectory analysis at 0600 UTC 4 August at a 3-km altitude in the area where convection initiates (Fig. 14c) using the Hybrid Single Particle Lagrangian Integrated Trajectory Model (HYSPLIT; Draxler and Rolph 2011) with 2.5° NCEP–National Center for Atmospheric Research (NCAR) reanalysis (Kalnay et al. 1996). It is obvious that the increase of moisture in northeast Guangdong area where convection was initiated is mainly due to the moisture transportation by the outer flow of the approaching Kammuri. As a result of increasing low-level moisture, CAPE (contours in Figs. 14a,b) increased substantially in the northeast Guangdong area, which completes all the necessary ingredients for the development of deep convection (moisture, lifting, and instability; Doswell et al. 1996). This result and the contribution of the TC to the maintenance of the pre-TC squall line by providing an environment favorable for the linear growth of the convection as proposed at the end of section 3e will be further confirmed through the following numerical simulations.

b. Numerical experiments

To further investigate possible impacts of Kammuri's approach on the formation and evolution of the pre-TC squall line, numerical experiments were performed using the Weather Research and Forecasting (WRF) model version 3.2 (Skamarock et al. 2008) with three domains and two-way nesting (Fig. 15). The model is integrated for 24 h starting at 0000 UTC 4 August 2008 with the initial and boundary conditions provided by 6-hourly FNL/NCEP analysis of 1° by 1°. The grid spacing of each domain is 40.5, 13.5, and 4.5 km. All domains have 35 vertical layers with the model top at 10 hPa. Physical parameterization schemes include Grell–Devenyi cumulus scheme (Grell and Devenyi 2002), WRF double-moment (WDM) six-class microphysics (Hong et al. 2010), and the Yonsei State University (YSU) scheme (Noh et al. 2003) for planetary boundary layer processes. No cumulus parameterization scheme was used in domain 3. All discussions are based on the results of domain 3.

As a result of a weaker initial TC, WRF simulation initialized with the FNL analysis at 0000 UTC 4 August develops a TC much weaker than observed. In this experiment, the convection dissipates rapidly though initiated under favorable synoptic forcing (not shown). To have an initial and evolving vortex similar to the reality especially from an intensity point of view, we used the TC-bogussing module in WRFV3.2 (Low-Nam and Davis 2001) for TC initialization. This bogussing

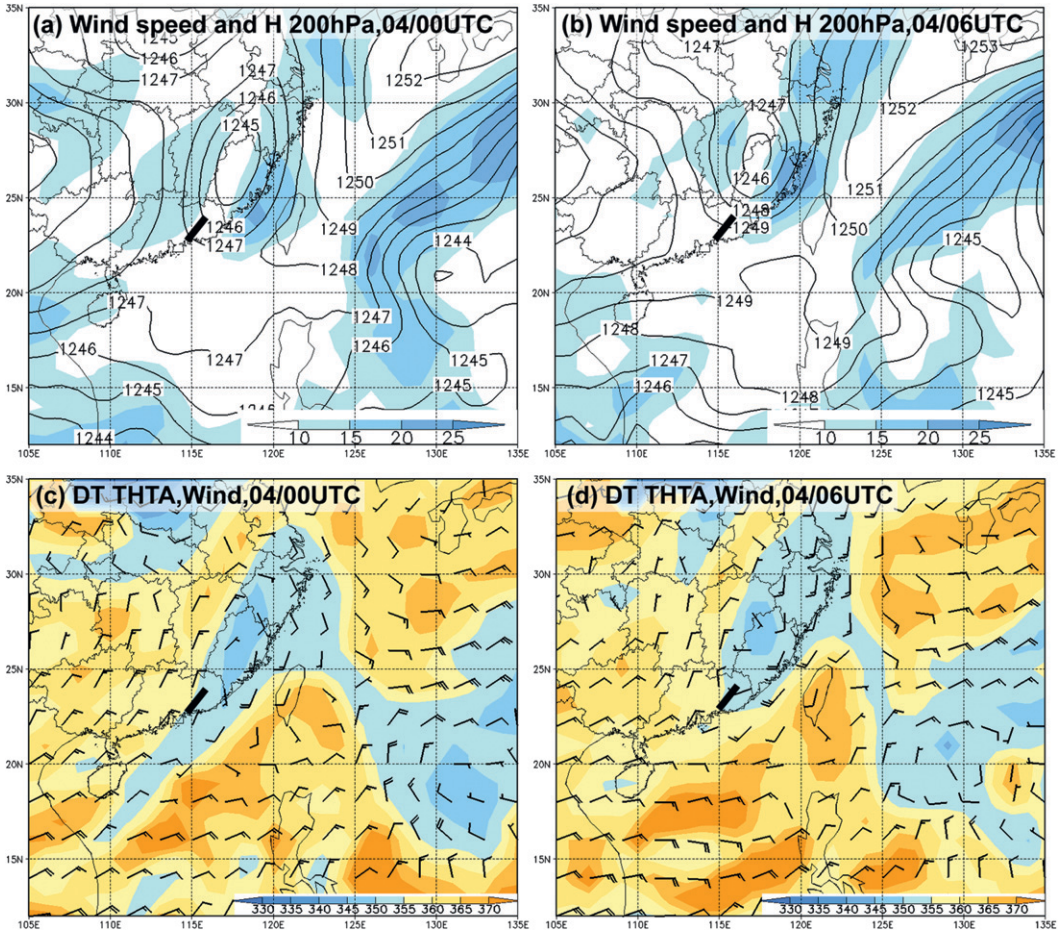

FIG. 12. 200-hPa wind speed (shaded according to the color bar in m s^{-1}) and geopotential height (solid contour every 10 gpm) at (a) 0000 and (b) 0600 UTC 4 Aug 2008. (c),(d) The dynamic tropopause (DT) potential temperature (shaded according to the color bar in K) and wind (full barb = 10 m s^{-1}) at 0000 and 0600 UTC 4 Aug 2008. The heavy short line denotes where the convection was initiated.

method is a two-step process, first removing the vortex from the analysis and then adding the bogus vortex. In the first step, vorticity and divergence are zeroed out respectively everywhere except for the vortex area to retrieve the nondivergent wind, the irrotational wind, the geopotential height anomaly, and the associated temperature anomaly. Then all these fields are removed from the first guess and finally relative humidity is adjusted. In the second step, adding a bogus TC using observed best-track information including location, a scaled maximum wind speed, and its radius is used to first define velocity potential and streamfunction, then to solve for geopotential height. Temperature is computed using the obtained geopotential height. Finally the relative humidity is modified.

At 0000 UTC 4 August (the initial time for model integration), Kammuri was still a tropical depression. The minimum SLP estimation is near 1000 hPa (available online at http://agora.ex.nii.ac.jp/digital-typhoon). No wind information is available at this stage. The maximum wind speed and its radius are chosen through a trial-and-error method using a series of sensitivity experiments to make the simulated TC match as close as possible to the observed TC intensity in addition to a well-simulated pre-TC squall line. The maximum wind speed we finally used is 12 m s^{-1} with a radius of 75 km, which will be referred to as the control experiment (CNTL). The evolution of the simulated minimum SLP is shown in Fig. 16.

Results suggest that Kammuri's presence may have helped to initiate the convection, the following linear organization of the convection, and the maintenance of the squall line (Figs. 17a,b) though the simulated squall line moves somewhat faster with a larger areal extent than observed. At 0500 UTC, a band of high CAPE extends northward from 21°N along 115°E (Fig. 18a).

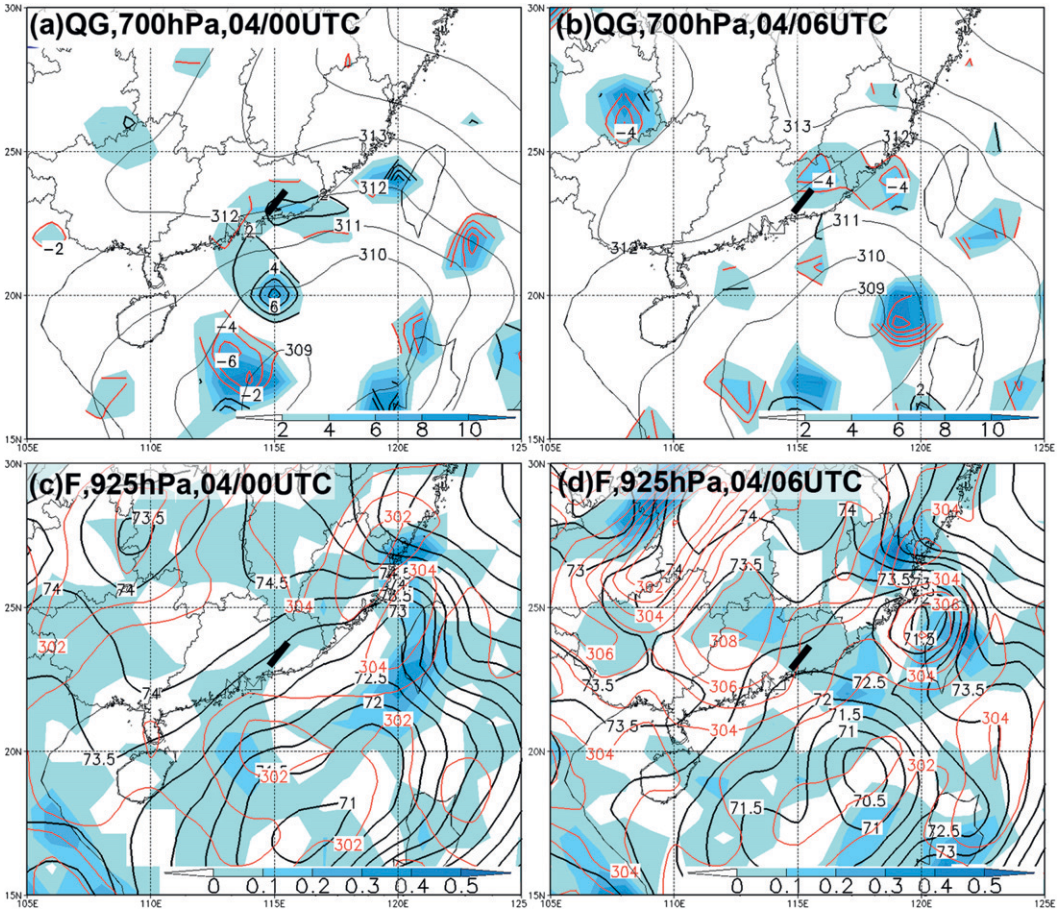

FIG. 13. The QG forcing for upward motion by summing the two terms on the right-hand side of the QG-omega equation (shaded every 1×10^{-19} m kg^{-1} s^{-1}; only positive values are plotted), the relative importance of vorticity and temperature advection (black for dominance of vorticity advection and red for dominance of temperature advection), and geopotential height (gray thin contour every 10 gpm) at 700 hPa at (a) 0000 UTC 4 Aug and (b) 0600 UTC 4 Aug 2008. The 925-hPa frontogenesis [shaded, 10^{-2} K km^{-1} (3 h)$^{-1}$], geopotential height (black contour every 10 gpm), and potential temperature (red contour every 1 K) are plotted at (c) 0000 UTC 4 Aug and (d) 0600 UTC 4 Aug 2008. The heavy short line denotes where the convection was initiated.

Collocated with this high-CAPE area are rich moisture and confluent flow at 925 hPa (Figs. 18b,c) oriented northeast-to-southwest from north Guangdong Province to about 21°N, 115°E providing a beneficial environment for the linear development of convection. A line of very weak echoes appear nearly along the border between Jiangxi and Fujian Provinces extending southward along 115°E to the coastal area (Fig. 19a) in this confluent flow. A strong echo appears on the coastal line of Guangdong province at 23°N, 116°E at 0530 UTC with the intensification of the line of weak echo (Fig. 19b). The weak echo line continues intensifying and extending southward to about 19°N, 114.5°E in the next hour (Figs. 19c,d), which is almost perpendicular to a spiral band of the TC. The above-mentioned strong echo on the coastal line substantially intensifies with new strong echoes developing next to it along the line while the weak echoes to the south of the strong convection dissipate. By 0730 UTC, a continuous 40-dBZ band oriented southwest-to-northeast has taken shape near the northern coastal area of Guangdong Province. The time and location of the formation of the squall line is very close to the observations (Fig. 10).

The maintenance and propagation of this squall line is in a suboptimal condition according to the Rottuno–Klemp–Weisman (RKW) theory (Rotunno et al. 1988). This theory argues that the optimum condition for the deep lifting at the leading edge of the cold pool (LECP) is that the environmental vertical shear normal to the LECP through the depth of the cold pool is equal to the horizontal vorticity generated by the LECP. This horizontal vorticity is the theoretical speed of the cold pool that can be calculated by

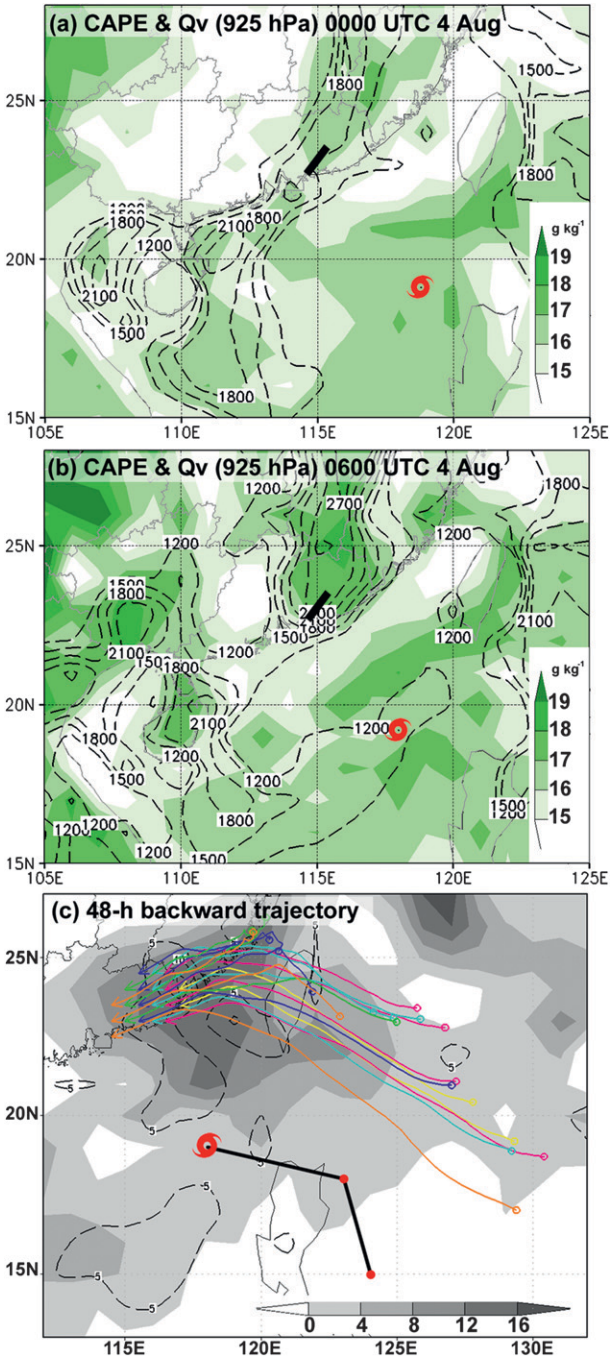

FIG. 14. Water vapor mixing ratio at 925 hPa (shaded; g kg^{-1}) and CAPE (contour; J kg^{-1}) at (a) 0000 UTC 4 Aug 2008 and (b) 0600 UTC 4 Aug 2008. The short heavy line in (a) and (b) stands for the orientation of linear growth of initial convection. The red typhoon mark denotes the center of Kammuri. (c) Also plotted are twenty 48-h backward trajectories from the area where the convection was initiated at 3-km altitude at 0600 UTC 4 Aug back to 0600 UTC 2 Aug 2008 (denoted by small circles). Different colors of the trajectories denote different longitudinal locations. The dashed lines represent the increase of relative humidity (every 5%) during the two days. The shaded area denotes the increase of precipitable water (every 4 kg m^{-2}).

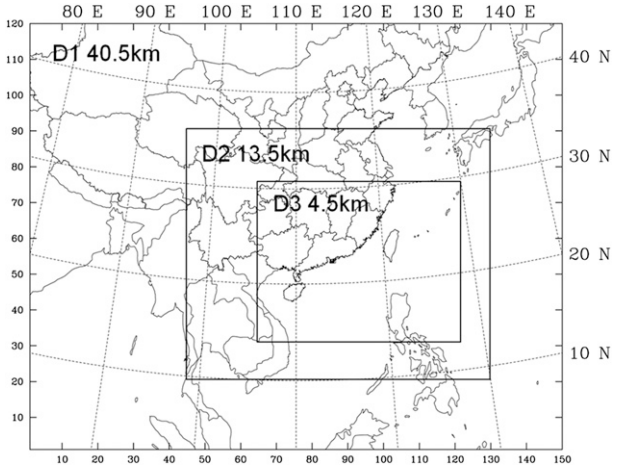

FIG. 15. Domains and their grid sizes of the numerical experiments.

$$c^2 = -2\int_{z=0}^{z=H} B\,dz, \tag{1}$$

where B is the total cold pool buoyancy including contributions from virtual potential temperature perturbations θ_v' and the mixing ratio of all condensate q_c, defined as $B = g(\theta_v'/\overline{\theta}_v - q_c)$. Here $\overline{\theta}_v$ is the environmental averaged virtual potential temperature. The ratio between c and the maximum environmental vertical shear normal to the LECP through the layer of the cold pool is $c/\Delta u = 1$ for an optimum condition. This theory has been confirmed by Weisman and Rotunno (2004) through a 3D simulation with a higher resolution and a larger range of environmental shear conditions than those in Weisman and Rotunno (2004) and it is also supported by a multimodel assessment (Bryan et al. 2006). The method we

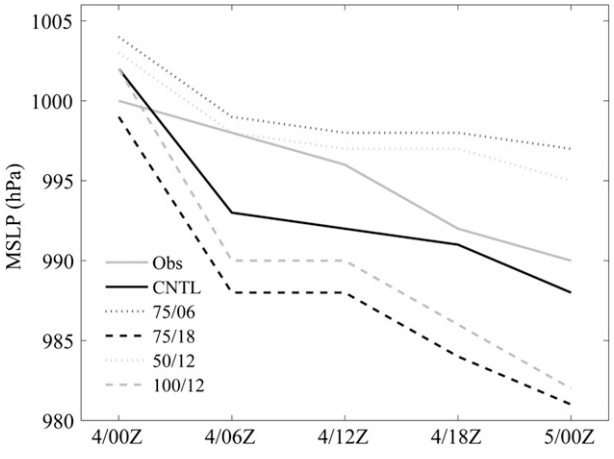

FIG. 16. Evolution of the intensity of Kammuri in terms of minimum SLP (hPa) in reality (available online at http://agora.ex.nii.ac.jp/digital-typhoon) and various sensitivity experiments.

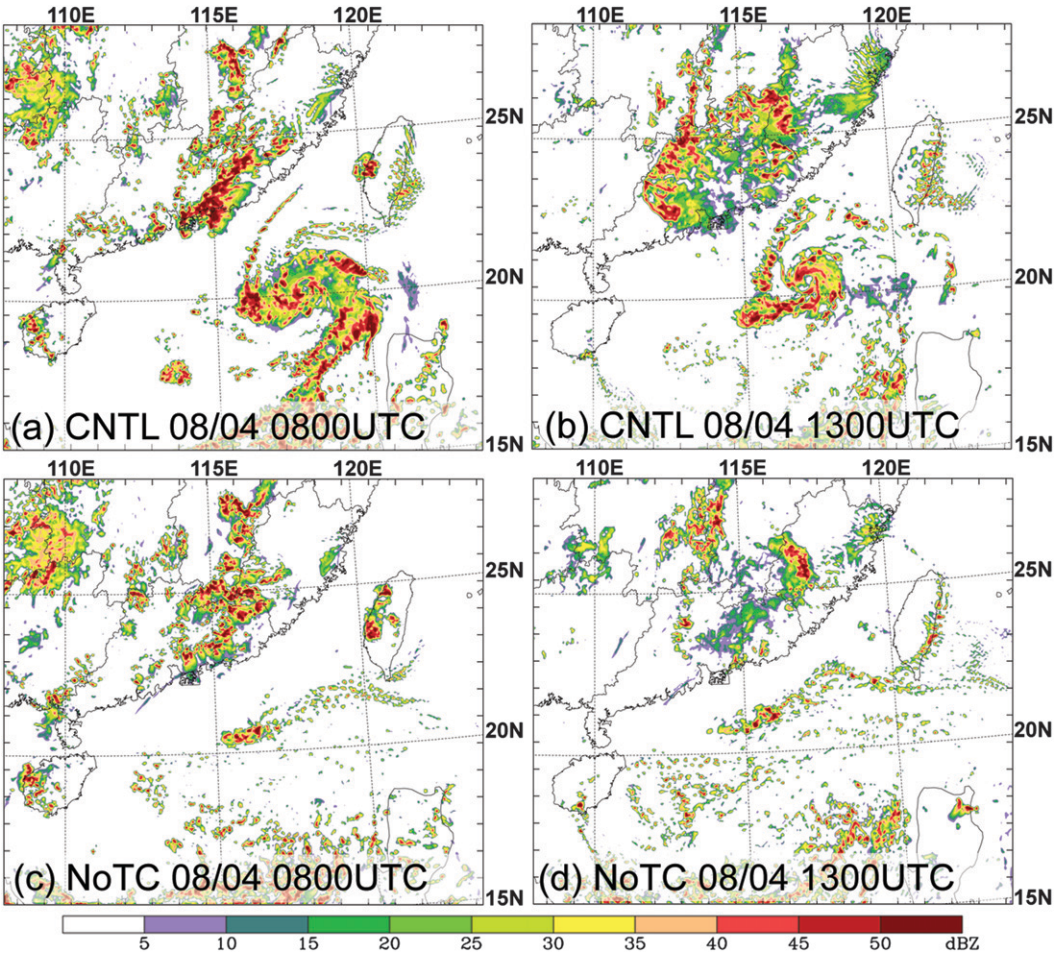

FIG. 17. The model composite radar reflectivity at (left) 0800 and (right) 1300 UTC 4 Aug for the (top) control experiment and (bottom) sensitivity experiment of NoTC.

used to calculate c and B is similar to Trier et al. (2006), except that H, the depth of the cold pool, is defined in this work as the depth of the layer where $\theta_v'(H) \leq 0$ K instead of $B(H) \leq 0$ because the vertical gradient of B near zero has a very large variability and may result in an unreasonably deep cold pool. Here $\overline{\theta}_v$ is calculated as an average of virtual potential temperature over a square area about 70 km ahead of the LECP with a length (width) of about 40 (20) km in the direction parallel (normal) to the LECP (area B in Fig. 20). The averaged virtual potential temperature in the cold pool $\overline{\theta}_c$ is an average of virtual potential temperature calculated at all points within an area about 10 km behind the LECP with a length (width) of about 40 (20) km in the direction parallel (normal) to the LECP (area C in Fig. 20). The perturbation virtual potential temperature is then obtained by $\overline{\theta}_c - \overline{\theta}_v$. The q_c is calculated in the same way as $\overline{\theta}_c$. Wind component normal to the LECP was calculated by projecting the ground relative wind vector at each level to the direction normal to the LECP at about 100 km ahead of the LECP (area V in Fig. 20). The maximum environmental vertical shear $\Delta u_{\max}$ is then obtained through H. The geometry used in above calculation is exactly the same as that in Trier et al. (2006, see their Fig. 9). The ratios of $c/\Delta u_{\max}$ at the developing and mature stages in the control experiment are 3.1 and 2.4, respectively, which is much larger than 1 likely due to the insufficient vertical shear in the TC environment. This suboptimal condition might have contributed to the dominant trailing-stratiform organization and the short life span of this pre-TC squall line.

However, when the weak TC circulation in the FNL analysis was removed via the first step of the TC bogussing method as described previously (hereafter referred to as NoTC), the early convection still appears but fails to organize into a squall line (Figs. 17c,d) without the supportive environment of the approaching TC. There are several potential reasons why the model fails to form a squall line when the TC is removed. First, CAPE is

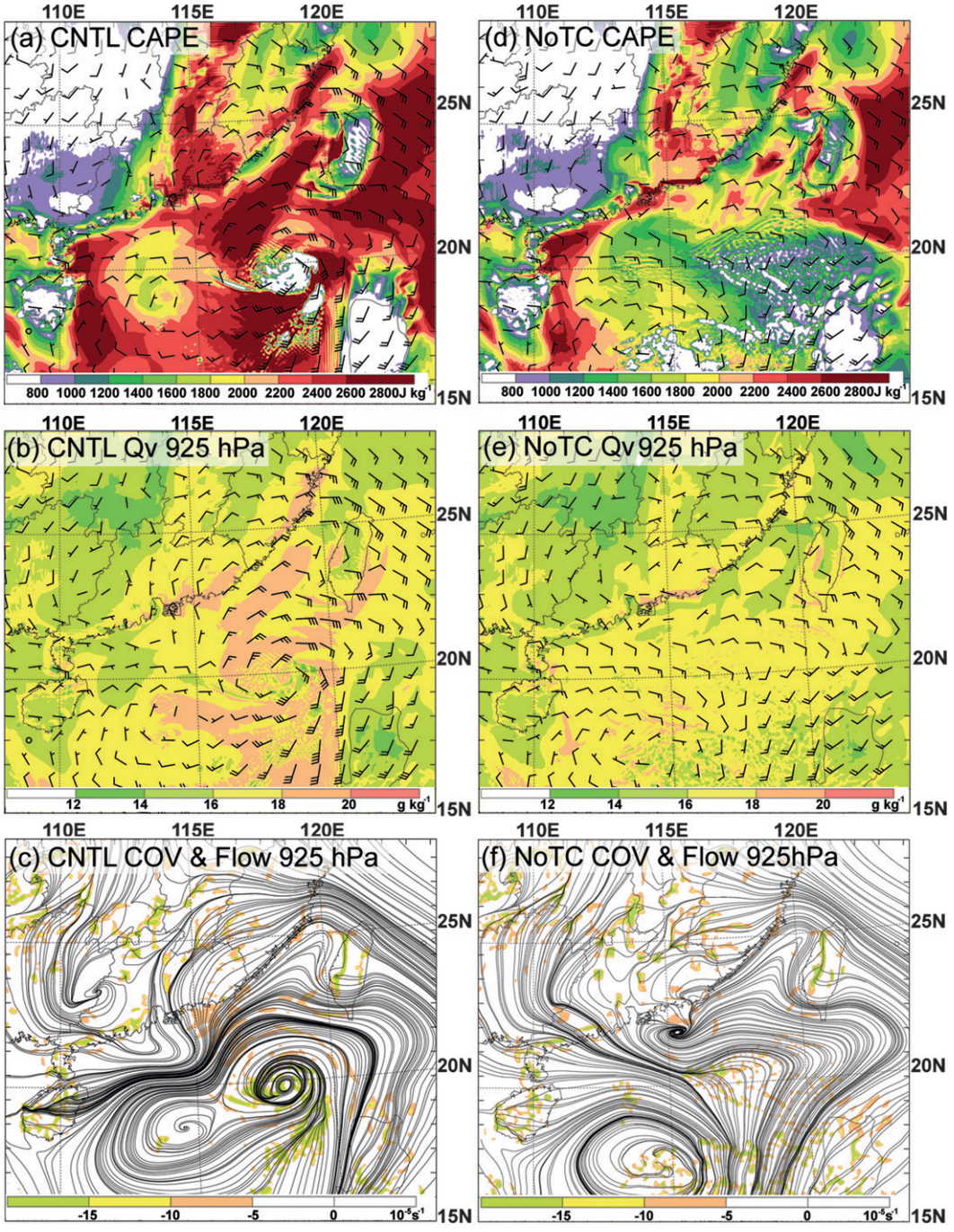

FIG. 18. (top) The simulated CAPE (shaded in J kg^{-1}), (middle) water vapor mixing ratio (shaded in g kg^{-1}) at 925 hPa, and (bottom) convergence (shaded in 10^{-5} s^{-1}) together with streamline at 925 hPa at 0500 UTC 4 Aug for the (left) control experiment and (right) sensitivity experiment NoTC. (a),(b),(d),(e) Wind vectors at 925 hPa (full barb = 5 m s^{-1}).

lower where the convection develops into a squall line in NoTC than in CNTL (Figs. 18a,d). Second, the water vapor mixing ratio at lower levels in NoTC is substantially reduced relative to that in the CNTL experiment (Figs. 18b,e) likely due to the smaller transportation of moisture toward the coastal area and eastern part of Guangdong Province by the TC. This could partially explain its less CAPE over the sea and near the coast of Guangdong Province. Third, the 0–3-km environmental vertical shear is apparently weaker by 1–4 m s^{-1} in the first several

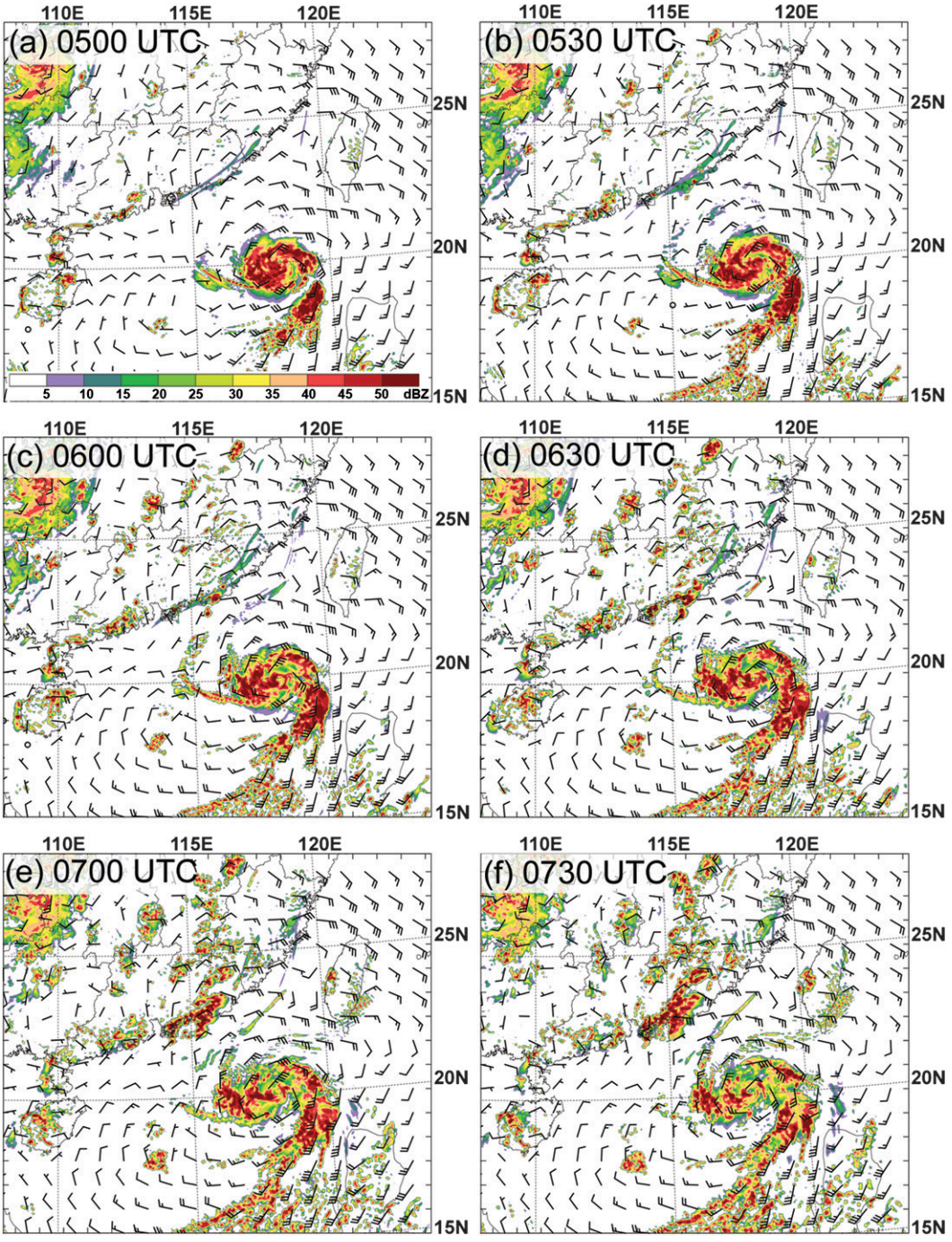

FIG. 19. The simulated composite radar reflectivity and wind barb at 925 hPa (full barb = 5 m s^{-1}) for the control experiment at (a) 0500, (b) 0530, (c) 0600, (d) 0630, (e) 0700, and (f) 0730 UTC 4 Aug 2008.

hours in the NoTC than that in the CNTL. The vertical shear increases gradually from 5 to 10 m s^{-1} in the CNTL while it keeps oscillating around 5 m s^{-1} in the NoTC. Besides, the 925-hPa convergence is smaller where the convection is supposed to organize into a squall line relative to that in the CNTL experiment (Figs. 18c,f), which reconfirmed that the approaching TC may have provided a favorable condition for the linear growth of convection and thus the formation of the squall line.

To examine the impact of the size and intensity of the approaching TC on the formation and evolution of the squall line, two sets of sensitivity experiments were

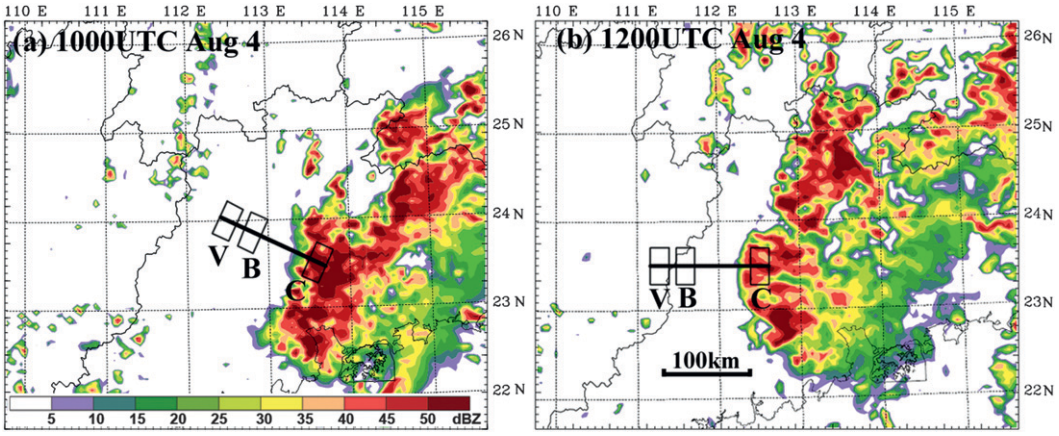

FIG. 20. The geometry used in the calculation of virtual potential temperature and buoyancy perturbation as well as the vertical wind profile normal to the leading edge of the squall line at its (a) developing and (b) mature stages. The background is the simulated composite radar reflectivity of the control experiment. Letters V and B denote the area used to calculate the averages of environmental wind and virtual temperature, and C is for the average of virtual temperature and condensates of the cold pool.

conducted by gradually changing the maximum wind and its radius. The first set was aimed to examine the sensitivity of the squall line to the maximum wind with the same radius including R75/W06 (the naming follows radius of the maximum wind in km/the maximum wind in m s^{-1}), R75/W12 (the CNTL experiment), and R75/W18. The second set was constructed to explore the impact of TC size on the preceding squall line including R50/W12, R75/W12 (the CNTL experiment), and R100/W12 (Fig. 21). The simulated evolution of the TC intensity of these four sensitivity experiments are shown in Fig. 16, which shows that either an increase in the maximum wind speed or its radius produced a stronger TC in terms of minimum SLP and vice versa. Figure 21 demonstrates that a larger and stronger TC tends to be beneficial for the development of a longer squall line. With the decrease of the maximum wind speed or its radius, the squall line gradually shrinks on its southern end. This case study is just aimed to provide an example of a pre-TC squall line and in what way the approaching TC could affect the formation and evolution of the pre-TC squall line. Detailed dynamic analysis on the interaction between a pre-TC squall line and the associated TC is beyond the scope of this paper.

5. Summary

This paper examines basic radar traits and surface and environmental features of squall lines preceding landfalling TCs in China based on the mosaic of composite radar reflectivity, surface, and radiosonde observations and FNL/NCEP analyses during 2007–09. We use a radar-reflectivity-based threshold to define squall lines following Parker and Johnson (2000). In particular, a quasi-contiguous 40-dBZ region must extend at least 100 km in length, last at least 3 h, and should be linear or quasi-linear while sharing a common leading edge. We examine only those squall lines that occur within the front quadrants of an approaching TC and are distinctly separate from the 20-dBZ reflectivity contour of the parent TC and its outer rainbands.

The statistics show that about 43% of landfalling TCs during 2007–09 were associated with pre-TC squall lines in China, and half of these TCs had multiple squall lines. Most pre-TC squall lines formed in August, from late afternoon to midnight, in the flat area of Guangdong province. About 70% of the pre-TC squall lines formed in a broken-line mode and 70% had a trailing-stratiform organizational pattern. The squall lines generally formed about 600 km ahead of their parent TC and about 36° to the right side of the TC track. They typically dissipated 640 km downstream at a smaller angle to the right side of the TC track. A bigger TC tends to be associated with a squall line more distant from the TC center. On average, the pre-TC squall lines had a maximum length of 224 km, a maximum radar reflectivity of 57–62 dBZ, a life span of 4 h, and moved at 12.5 m s^{-1}. Compared with midlatitude squall lines, the lifetime and length of pre-TC squall lines are shorter, though the translation speed is similar. Relative to the subtropical squall lines, pre-TC squall lines have a similar maximum length and moving speed, a stronger intensity and a shorter life span. Relative to the squall line in north China, the pre-TC squall line shows a shorter life span and slower-moving speed with a similar maximum length.

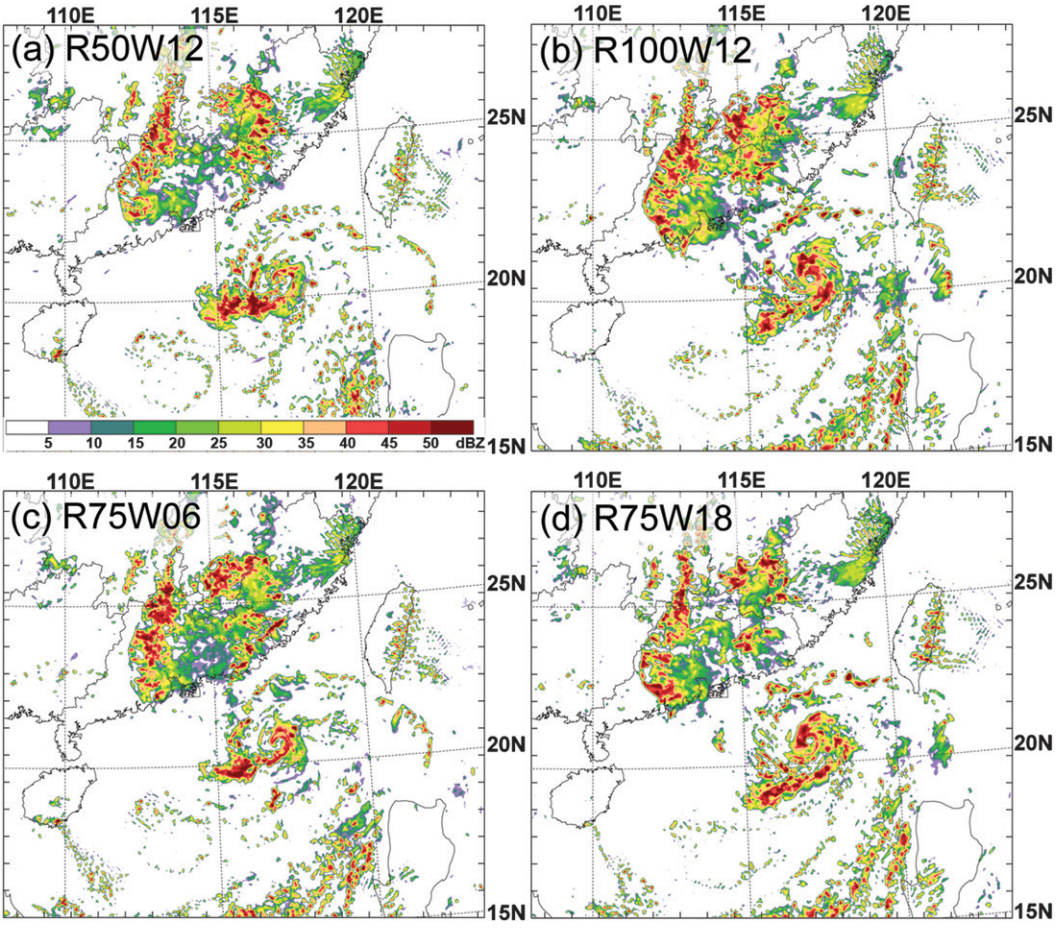

FIG. 21. The simulated composite radar reflectivity for the sensitivity experiments (a) R50W12, (b) R100W12, (c) R75W06, and (d) R75W18 at 1300 UTC 4 Aug.

Surface features of these pre-TC squall lines were examined using hourly surface observation including the range and median of mean SLP, potential temperature, wind, and hourly rainfall. Relative to the MCSs in midlatitude, the pre-TC squall lines were associated with weaker pressure rises (1.2 vs 3.6 hPa) and smaller decreases in potential temperature (6.2 vs 9.8 K). The smaller changes of temperature, pressure, and wind speed indicate a weaker cold pool in pre-TC squall lines relative to their midlatitude counterpart. The weaker cold pool of the pre-TC squall line is likely related to the presence of deep moisture from the TC that mitigates the production of cold downdrafts. The moister environment of pre-TC squall lines relative to typical midlatitude and subtropical MCSs is also demonstrated in the lower LCL and higher precipitable water.

Analyses on the radiosondes representing the prestorm environment of pre-TC squall lines show that conditional instability is smaller than for spring-season squall lines in Oklahoma, but larger than prefrontal squall lines averaged across the whole contiguous United States and subtropical squall lines. Consistent with midlatitude and fast-moving tropical squall lines, the 0–3-km vertical shear in the environment where the pre-TC squall lines form has a dominant component normal to the long axis of squall lines with a smaller magnitude of about 8 m s^{-1} with respect to their midlatitude and subtropical counterparts.

The role of the parent TC in the formation of its preceding squall line is examined through a case study. Results show that the approach of the parent TC may help to transform the environment into one that can support a squall line given some external forcing for convection via providing rich moisture and low-level convergence. With the removal of the TC, the convection was still initiated but was more scattered, failed to organize into a long-lasting squall line, and dissipated rapidly likely due to the reduced instability, moisture, and low-level convergence. Sensitivity experiments also show that a stronger or a larger TC is beneficial to the formation of a longer squall line.

In summary, the synoptic and numerical experiment results shown herein indicate that pre-TC squall lines may go through the following process: there exists a synoptic environment favorable for convective initiation including high instability, moisture, and lifting by low-level mesoscale frontogenesis and/or surface convergence. Different from its role in PREs, the synoptic lifting may be unimportant in directly forcing the initiation of convection, but may help to prime an environment favorable for the development of convection by decreasing CIN and increasing CAPE. The convection then organizes into a linear shape along the confluent region between the outer flow of the TC and its neighboring system. The approaching TC helps to maintain the squall line through providing rich moisture and linear lifting in a suboptimal condition with a ratio between the vorticity associated with the cold pool and the environmental vertical shear through the depth of the cold pool much larger than $c/\Delta u = 1$.

Because of the limited database, the sample size of the pre-TC squall lines is small, so the result maybe not statistically significant. However, from these 17 cases, we get a general idea on the behavior of pre-TC squall lines, such as their formation frequency, geographical and temporal distribution, basic radar signatures, surface and environment features, their possible relationship with the approaching TCs, and their possible differences from the midlatitude prefrontal and subtropical squall lines. This should be helpful for the operational forecast of TC-associated severe weather. Additionally, this paper shows only the sensitivity of a pre-TC squall line to the size and intensity of the associated TC. Other aspects worthy of being explored include detailed dynamics of how the TC affects its preceding squall line, the role of coastal topography on the formation and evolution on the pre-TC squall line, and the feedback of the pre-TC squall line to the associated TC. We will look to address these issues in future works.

Acknowledgments. We thank Fuqing Zhang (PSU) and Jason Sippel (NASA/GSFC) for their constructive comments and the insightful discussions with them on this work. Additional thanks also go to the editor, George Bryan (NCAR), and two anonymous reviewers for their valuable comments. The radar mosaics were made available by Chinese National Meteorological Center. This research is sponsored by China National Basic Research Program 2009CB421504 (China), and Grants NSFC41075031, NSFC40921160380, and NSFC40730948.

REFERENCES

Barnes, G. M., and K. Sieckman, 1984: The environment of fast- and slow-moving tropical mesoscale convective cloud lines. *Mon. Wea. Rev.,* **112,** 1782–1794.

Bluestein, H. B., and M. H. Jain, 1985: Formation of mesoscale lines of precipitation: Severe squall lines in Oklahoma during the spring. *J. Atmos. Sci.,* **42,** 1711–1732.

Bryan, G. H., J. C. Knievel, and M. D. Parker, 2006: A multimodel assessment of RKW Theory's relevance to squall-line characteristics. *Mon. Wea. Rev.,* **134,** 2772–2792.

Chen, G. T.-J., and H.-C. Chou, 1993: General characteristics of squall lines observed in TAMEX. *Mon. Wea. Rev.,* **121,** 726–733.

Dial, G. L., J. P. Racy, and R. L. Thompson, 2010: Short-term convective mode evolution along synoptic boundaries. *Wea. Forecasting,* **25,** 1430–1446.

Ding, Y.-H., H.-Z. Li, M.-L. Zhang, J.-S. Li, and Z.-Y. Cai, 1982: A study on the formation condition of squall line in China (in Chinese). *Chin. J. Atmos. Sci.,* **6,** 18–27.

Doswell, C. A., III, H. E. Brooks, and R. A. Maddox, 1996: Flash flood forecasting: An ingredients-based methodology. *Wea. Forecasting,* **11,** 560–581.

Draxler, R. R., and G. D. Rolph, cited 2011: HYSPLIT (HYbrid SingleParticle Lagrangian Integrated Trajectory) Model. NOAA/Air Resources Laboratory, Silver Spring, MD. [Available online at http://ready.arl.noaa.gov/HYSPLIT.php.]

Engerer, N. A., D. J. Stensrud, and M. C. Coniglio, 2008: Surface characteristics of observed cold pools. *Mon. Wea. Rev.,* **136,** 4839–4849.

Evans, J. S., and C. A. Doswell III, 2001: Examination of derecho environments using proximity soundings. *Wea. Forecasting,* **16,** 329–342.

Galarneau, T. J., Jr., L. F. Bosart, and R. S. Schumacher, 2010: Predecessor rain events ahead of tropical cyclones. *Mon. Wea. Rev.,* **138,** 3272–3297.

Gao, S., Z. Meng, F. Zhang, and L. F. Bosart, 2009: Observational analysis of heavy rainfall mechanisms associated with severe Tropical Storm Bilis (2006) after its landfall. *Mon. Wea. Rev.,* **137,** 1881–1897.

Geerts, B., 1998: Mesoscale convective systems in the Southeast United States during 1994–95: A survey. *Wea. Forecasting,* **13,** 860–869.

Grell, G. A., and D. Devenyi, 2002: A generalized approach to parameterizing convection combining ensemble and data assimilation techniques. *Geophys. Res. Lett.,* **29,** 1693–1696.

He, H., and F. Zhang, 2010: Diurnal variations of warm-season precipitation over northern China. *Mon. Wea. Rev.,* **138,** 1017–1025.

Hong, S.-Y., K.-S. Sunny Lim, Y.-H. Lee, J.-C. Ha, H.-W. Kim, S.-J. Ham, and J. Dudhia, 2010: Evaluation of the WRF double-moment 6-class microphysics scheme for precipitating convection. *Adv. Meteor.,* **2010,** 707253, doi:10.1155/2010/707253.

Houze, R. A., Jr., 1977: Structure and dynamics of a tropical squall–line system. *Mon. Wea. Rev.,* **105,** 1540–1567.

——, 1993: *Cloud Dynamics*. Academic Press, 573 pp.

——, B. F. Smull, and P. Dodge, 1990: Mesoscale organization of springtime rainstorms in Oklahoma. *Mon. Wea. Rev.,* **118,** 613–654.

James, R. P., J. M. Fritsch, and P. M. Markowski, 2005: Environmental distinctions between cellular and slabular convective lines. *Mon. Wea. Rev.,* **133,** 2669–2691.

Kalnay, E., and Coauthors, 1996: The NCEP/NCAR 40-Year Reanalysis Project. *Bull. Amer. Meteor. Soc.,* **77,** 437–471.

Li, H.-Z., 1988: Features of squall lines on regional surface weather map and their nowcasting in North China (in Chinese). *Chin. J. Atmos. Sci.,* **12,** 42–48.

Low-Nam, S., and C. Davis, 2001: Development of a tropical cyclone bogussing scheme for the MM5 system. Preprints, *11th*

PSU/NCAR Mesoscale Model Users' Workshop, Boulder, CO, PSU/NCAR, 130–134.

Noh, Y., W.-G. Cheon, S.-Y. Hong, and S. Raasch, 2003: Improvement of the K-profile model for the planetary boundary layer based on large eddy simulation data. *Bound.-Layer Meteor.,* **107,** 401–427.

Parker, M. D., and R. H. Johnson, 2000: Organizational modes of midlatitude mesoscale convective systems. *Mon. Wea. Rev.,* **128,** 3413–3436.

Powell, M. D., 1990: Boundary layer structure and dynamics in outer hurricane rainbands. Part I: Mesoscale rainfall and kinematic structure. *Mon. Wea. Rev.,* **118,** 891–917.

Rotunno, R., J. B. Klemp, and M. L. Weisman, 1988: A theory for strong, long-lived squall lines. *J. Atmos. Sci.,* **45,** 463–485.

Schumacher, R. S., T. J. Galarneau Jr., and L. F. Bosart, 2011: Distant effects of a recurving tropical cyclone on rainfall in a midlatitude convective system: A high-impact predecessor rain event. *Mon. Wea. Rev.,* **139,** 650–667.

Skamarock, W. C., and Coauthors, 2008: A description of the Advanced Research WRF version 3. NCAR Tech. Note TN-475_STR, 113 pp.

Steiner, M., R. A. Houze Jr., and S. E. Yuter, 1995: Climatological characterization of three-dimensional storm structure from operational radar and rain gauge data. *J. Appl. Meteor.,* **34,** 1978–2007.

Trier, S. B., C. A. Davis, D. A. Ahijevych, M. L. Weisman, and G. H. Bryan, 2006: Mechanisms supporting long-lived episodes of propagating nocturnal convection within a 7-day WRF model simulation. *J. Atmos. Sci.,* **63,** 2437–2461.

Wallace, J. M., 1975: Diurnal variations in precipitation and thunderstorm frequency over the conterminous United States. *Mon. Wea. Rev.,* **103,** 406–419.

Weisman, M. L., and R. Rotunno, 2004: ''A theory for strong long-lived squall lines'' revisited. *J. Atmos. Sci.,* **61,** 361–382.

Wyss, J., and K. A. Emanuel, 1988: The pre-storm environment of midlatitude prefrontal squall lines. *Mon. Wea. Rev.,* **116,** 790–794.